

Photometric and Polarimetric Signatures of Geosynchronous Satellites

Daniel Jones

A senior thesis submitted to the faculty of  
Brigham Young University  
in partial fulfillment of the requirements for the degree of  
Bachelor of Science

J. Ward Moody, Advisor

Department of Physics and Astronomy  
Brigham Young University

Copyright © 2019 Daniel Jones

All Rights Reserved

## ABSTRACT

### Photometric and Polarimetric Signatures of Geosynchronous Satellites

Daniel Jones

Department of Physics and Astronomy, BYU

Bachelor of Science

Geosynchronous satellites (GEOs) need to be monitored to track their health, effects of space aging, and unexpected maneuvers. This can be accomplished by creating photometric and polarimetric signatures from light curves. To develop our understanding about how the light curves reveal the needed information, we began by studying the 101 W satellite cluster. To create the light curves, observations were taken through Johnson V, B, R, and I filters as well as polarized filters using the telescopes at the Remote Observatory for Variable Object Research (ROVOR) in Delta, UT and at the Optical Delving Infrared iNnovation (ODIN) laboratory at the Kirtland Airforce Base in Albuquerque, NM. To determine the effects of aging, three signatures were compared with archived data for the respective GEOs. We found that dimming and/or reddening occurred. The dimming was equal to 0.1-0.2 mags and the B-V color increased by about 0.1 indicating a reddening by that amount. Using the polarized data, the Stokes parameters were calculated. An increased understanding of the satellite's structure and movements can be obtained by analyzing how these parameters change in a night.

Keywords: Polarimetry, Photometry, Geosynchronous satellites

## ACKNOWLEDGMENTS

First and foremost I would like to acknowledge the help and support of Dr. J Moody. His guidance throughout the research process for this work was invaluable. It was also through using his ROVOR telescope that much of the data were able to be collected. In addition to Dr. J Moody, I must also acknowledge the efforts of Scott Milster. It is his work at the Air Force Research Laboratories that initially brought this project to my attention. Along the way he too has been mentor and has advised me on ways to advance the research presented in this thesis.

# Contents

<b>Table of Contents</b>	<b>iv</b>
<b>List of Figures</b>	<b>vi</b>
<b>List of Tables</b>	<b>viii</b>
<b>1 Introduction</b>	<b>1</b>
1.1 Significance of Signatures . . . . .	1
1.2 Light Curves as Signatures for Geosynchronous Satellites . . . . .	3
1.3 Work Currently Being Done Elsewhere . . . . .	5
1.4 Major Findings . . . . .	7
1.5 Overview . . . . .	9
<b>2 Methods</b>	<b>10</b>
2.1 Satellite System Geometry . . . . .	10
2.2 Options for Studying Geosynchronous Satellites . . . . .	11
2.3 Photometric Methods Used . . . . .	12
2.4 Polarimetric Methods Used . . . . .	18
<b>3 Results and Conclusions</b>	<b>23</b>
3.1 Photometric Evidence of Space Aging . . . . .	23
3.2 Key Features in Polarimetric Data . . . . .	30
3.2.1 Polarimetry of DirecTV 9S . . . . .	30
3.2.2 Polarimetry of SES 1 . . . . .	33
3.2.3 Polarimetry of DirecTV 8 . . . . .	36
3.2.4 Polarimetry of DirecTV 4 . . . . .	38
3.3 Conclusion . . . . .	39
3.4 Further Work Needed . . . . .	41
<b>Appendix A Additional Satellite Plots</b>	<b>43</b>
A.1 DirecTV 9S Plots . . . . .	43
A.2 SES 1 Plots . . . . .	52

---

A.3 DirecTV 8 Plots . . . . .	61
<b>Bibliography</b>	<b>69</b>
<b>Index</b>	<b>70</b>
<b>Index</b>	<b>70</b>

# List of Figures

1.1	Satellites in Field of View of DirecTV 10 . . . . .	2
2.1	GEO schematic . . . . .	11
2.2	ROVOR Throughput . . . . .	20
2.3	Polarization Ellipse . . . . .	21
3.1	AMC 15 Space Aging . . . . .	24
3.2	AMC 15 Color Plot . . . . .	25
3.3	DirecTV 8 Space Aging . . . . .	26
3.4	DirecTV 8 Color Plot . . . . .	27
3.5	Spaceway 1 Space Aging . . . . .	28
3.6	Spaceway 1 Color Plot . . . . .	29
3.7	DirecTV 9S Polarization Data . . . . .	31
3.8	SES 1 Polarization Data . . . . .	34
3.9	DirecTV 8 Polarization Data . . . . .	37
3.10	DirecTV 4 Polarization Data . . . . .	38
A.1	DirecTV 9S counts for 28 October 2017 . . . . .	43
A.2	DirecTV 9S $S_1$ and $S_2$ polarization fractions for 28 October 2017 . . . . .	44
A.3	DirecTV 9S eccentricity and position angle for 28 October 2017 . . . . .	44

---

A.4	DirectTV 9S counts for 7 February 2018 . . . . .	45
A.5	DirectTV 9S $S_1$ and $S_2$ polarization fractions for 7 February 2018 . . . . .	45
A.6	DirectTV 9S eccentricity and position angle for 7 February 2018 . . . . .	46
A.7	DirectTV 9S counts for 16 February 2018 . . . . .	46
A.8	DirectTV 9S $S_1$ and $S_2$ polarization fractions for 16 February 2018 . . . . .	47
A.9	DirectTV 9S eccentricity and position angle for 16 February 2018 . . . . .	47
A.10	DirectTV 9S counts for 9 April 2018 . . . . .	48
A.11	DirectTV 9S $S_1$ and $S_2$ polarization fractions for 9 April 2018 . . . . .	48
A.12	DirectTV 9S eccentricity and position angle for 9 April 2018 . . . . .	49
A.13	DirectTV 9S counts for 25 May 2018 . . . . .	49
A.14	DirectTV 9S $S_1$ and $S_2$ polarization fractions for 25 May 2018 . . . . .	50
A.15	DirectTV 9S eccentricity and position angle for 25 May 2018 . . . . .	50
A.16	DirectTV 9S counts for 7 June 2018 . . . . .	51
A.17	DirectTV 9S $S_1$ and $S_2$ polarization fractions for 7 June 2018 . . . . .	51
A.18	DirectTV 9S eccentricity and position angle for 7 June 2018 . . . . .	52
A.19	SES 1 counts for 28 October 2017 . . . . .	52
A.20	SES 1 $S_1$ and $S_2$ polarization fractions for 28 October 2017 . . . . .	53
A.21	SES 1 eccentricity and position angle for 28 October 2017 . . . . .	53
A.22	SES 1 counts for 7 February 2018 . . . . .	54
A.23	SES 1 $S_1$ and $S_2$ polarization fractions for 7 February 2018 . . . . .	54
A.24	SES 1 eccentricity and position angle for 7 February 2018 . . . . .	55
A.25	SES 1 counts for 16 February 2018 . . . . .	55
A.26	SES 1 $S_1$ and $S_2$ polarization fractions for 16 February 2018 . . . . .	56
A.27	SES 1 eccentricity and position angle for 16 February 2018 . . . . .	56
A.28	SES 1 counts for 9 April 2018 . . . . .	57

---

A.29 SES 1 $S_1$ and $S_2$ polarization fractions for 9 April 2018 . . . . .	57
A.30 SES 1 eccentricity and position angle for 9 April 2018 . . . . .	58
A.31 SES 1 counts for 25 May 2018 . . . . .	58
A.32 SES 1 $S_1$ and $S_2$ polarization fractions for 25 May 2018 . . . . .	59
A.33 SES 1 eccentricity and position angle for 25 May 2018 . . . . .	59
A.34 SES 1 counts for 7 June 2018 . . . . .	60
A.35 SES 1 $S_1$ and $S_2$ polarization fractions for 7 June 2018 . . . . .	60
A.36 SES 1 eccentricity and position angle for 7 June 2018 . . . . .	61
A.37 DirecTV 8 counts for 7 February 2018 . . . . .	61
A.38 DirecTV 8 $S_1$ and $S_2$ polarization fractions for 7 February 2018 . . . . .	62
A.39 DirecTV 8 eccentricity and position angle for 7 February 2018 . . . . .	62
A.40 DirecTV 8 counts for 16 February 2018 . . . . .	63
A.41 DirecTV 8 $S_1$ and $S_2$ polarization fractions for 16 February 2018 . . . . .	63
A.42 DirecTV 8 eccentricity and position angle for 16 February 2018 . . . . .	64
A.43 DirecTV 8 counts for 9 April 2018 . . . . .	64
A.44 DirecTV 8 $S_1$ and $S_2$ polarization fractions for 9 April 2018 . . . . .	65
A.45 DirecTV 8 eccentricity and position angle for 9 April 2018 . . . . .	65
A.46 DirecTV 8 counts for 25 May 2018 . . . . .	66
A.47 DirecTV 8 $S_1$ and $S_2$ polarization fractions for 25 May 2018 . . . . .	66
A.48 DirecTV 8 eccentricity and position angle for 25 May 2018 . . . . .	67
A.49 DirecTV 8 counts for 7 June 2018 . . . . .	67
A.50 DirecTV 8 $S_1$ and $S_2$ polarization fractions for 7 June 2018 . . . . .	68
A.51 DirecTV 8 eccentricity and position angle for 7 June 2018 . . . . .	68

# List of Tables

2.1 Observations . . . . .	13
----------------------------	----

# Chapter 1

## Introduction

### 1.1 Significance of Signatures

There are currently 402 geosynchronous satellites in orbit around the Earth. With so many satellites that are in various stages of their lifetime, it becomes necessary to monitor them. This is one of the goals of Space Situational Awareness (SSA). To accomplish the aims of SSA it is essential to identify any unknown satellites and their capabilities. In addition to this, several details that need to be tracked for a satellite include its position, any maneuvers made, and the effects of space aging.

When looking at space aging, the goal is to quantify its effects, for individual satellites. These effects can be studied by looking at the light reflected off the satellite. As a satellite ages the solar panels will become more pitted which increases how much the the light is scattered. This means that less light will reach an observer and it will appear dimmer. The second expected effect is reddening of the reflected light. This means that when it is observed, more red or longer wavelengths of light will be seen instead of blue, short wavelengths. The greatest difficulty in quantifying these effects is that the materials will determine how the satellite ages over time.

Another problem that is growing as a result of more satellites being in orbit is cross tagging.

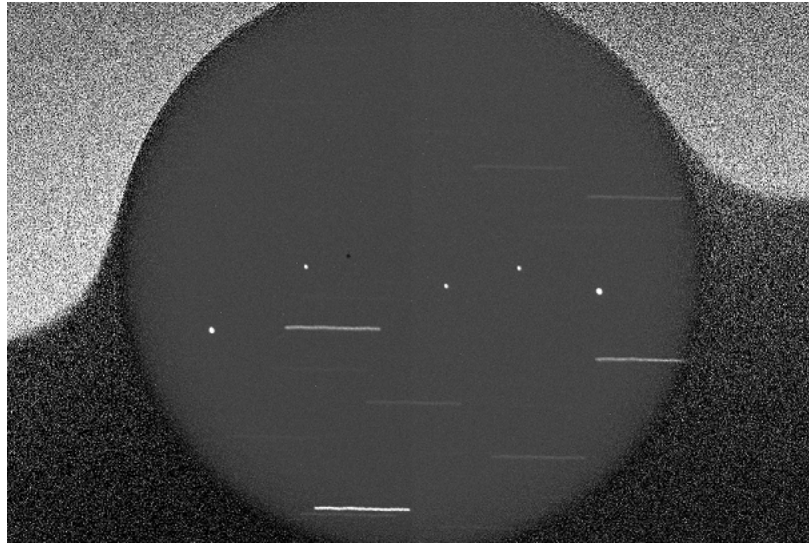


**Figure 1.1** A frame taken of DirecTV 10 and other satellites within a single field of view using the 14" telescope at the ODIN Laboratory. Light points are five geosynchronous satellites while the streaks of light are from stars in the field of view.

This occurs when two or more close satellites cannot be uniquely identified. For example, Figure 1.1 shows a frame from the 14-inch telescope at the ODIN Laboratory located at Kirkland Air Force Base in Albuquerque, New Mexico. The telescope was pointed at DirecTV 10, but within the field of view of the telescope there are four other satellites. Given this, it is difficult to correctly identify which satellite is DirecTV 10.

The first solution would be to directly image the satellites using a large telescope. This idea has two major problems. The first is that large telescopes are expensive to use and their observation time is extremely valuable. The second issue is that geosynchronous satellites orbit over 22,000 miles above the Earth and they are not large structures. So even with a large telescope and adaptive optics it is unlikely that the satellites could be imaged at all. Due to these two major challenges, other methods must be employed in order to achieve the aims previously mentioned.

## 1.2 Light Curves as Signatures for Geosynchronous Satellites

One solution is to use standard photometric and polarimetric procedures that are used in astronomy to study distant objects. Photometry simply means looking at the amount of light that is coming from an object. Similarly, polarimetry looks at the degree the light is polarized and whether it is circularly, elliptically, or linearly polarized. These methods are effective because factors like composition and the satellite structure will affect how bright the satellite appears and how the light is polarized.

The first factor that comes into play is how light is hitting the satellite. Like the moon, geosynchronous satellites reflect the light of the sun. Throughout the course of the night the angle between the satellite and the sun will change as the Earth rotates. The angle that the sun, Earth, and satellite make is defined as the phase angle. The phase angle is defined as being  $0^\circ$  when they are lined up, negative before this occurs, and positive afterwards. Generally, we only observe the satellite when the phase angle is between  $\pm 90^\circ$ . As the phase angle changes so will the apparent brightness of the satellite with the satellite being the brightest near  $0^\circ$  phase angle.

Another factor that will change how bright the satellite appears is its composition. The various materials used will reflect and scatter different amounts of light. In addition to this, they will not scatter or reflect all of the wavelengths of light equally. For example, solar panels appear blue because they tend to reflect more blue light than red. To account for this, we observed the satellites using color filters. Specifically, for this research the satellites were observed using the Johnson B, V, R, and I filters which measure the amount of light in the blue, visible, red, and near infrared wavelength regions.

Finally, the third aspect about the satellite that will affect how bright they appear throughout the night is their structure. According to the first Optical Delving Infrared iNnovation (ODIN) technical report by Moody et al., antennas, dishes, and other equipment break the symmetry of the satellite, and at various points throughout the night reflections off these structures can change the satellites'

brightness (Moody et al. 2018). Since these components are also going to be composed of different materials than the main satellite structure there will be additional differences in the brightness in the color filters.

Given these factors, studying satellites using photometric and polarimetric procedures is useful. Throughout the night, light measurements are taken with a telescope and CCD using the Johnson filters. The number of photometric counts from the satellite at a certain phase angle in one of the filters is recorded by the CCD. These counts are then plotted versus the phase angle and the result is a light curve for the satellite. Since the satellites have different main and additional structures as well as different materials, the light curves created will be unique to the satellite. For this reason, the light curve is thought to be a signature for a given satellite.

The light curves will also reflect changes in the satellites orientation as well as the effects of aging. If a satellite rotates or changes its general position, light will be reflected off differently and this can be seen as different features in the light curves appear or disappear. If during the satellites aging process reddening occurs, this will be manifested by a decrease in the counts in the blue filter throughout the night. Likewise, if the satellite dims over time this will be seen by the counts dropping uniformly across the night while the overall signature shape remains the same.

Similarly, by using polarized filters, light curves can be created for the satellites which show their brightness in various polarization angles as a function of phase angle. By using the counts per second, or the flux, received in these filters it is possible to determine the Stokes parameters which help define how the light is polarized. These parameters define the degree of polarization, the ellipticity of the polarization ellipse, and the orientation of ellipse (Moody et al. 2018). With the Stokes parameters, additional information about the structure and orientation of the satellite can be determined as well.

## 1.3 Work Currently Being Done Elsewhere

Given the importance of being able to classify and monitor satellites, research has been and is currently being done by other groups and organizations outside of Brigham Young University. The goals of this research are to refine and improve the methods being used. The first organization is the Air Force Research Laboratory (AFRL) in Albuquerque, New Mexico. I collected most of the photometric data during a summer internship with AFRL. The primary objective during this time was to be able to determine the effects of space aging. Near the end of the summer, we obtained polarized filters so that we could start collecting polarimetric data as well. The photometric data will be presented in Chapter 3 along with an analysis of the findings. Since the polarized filters arrived late in the summer there was very little time to obtain polarimetric data. However, future work with the AFRL will be focused on gathering polarimetric data on a number of geosynchronous satellites and analyzing it with the hope of being able to characterize these satellites.

Over the past few years, polarimetry research has been presented at the annual Advance Maui Optical and Space Surveillance (AMOS) Technologies Conference. One technical paper by Pasqual et al. focuses on active polarimetry in order to identify orbital debris. Their research made use of active polarimetry where “a target is illuminated by a laser with a variable, but controlled, polarization state” and then measurements about the reflected light are taken (Pasqual et al. 2015).

The purpose of the research done by Pasqual et al. was to be able to study three properties of various materials that compose satellites and debris. These properties are diattenuation, retardance, and depolarization. The diattenuation indicates how strongly the material reflects some polarization states relative to others and ranges from 0 to 1. The retardance is the relative phase shift between polarization states induced by the material. Lastly, the depolarization indicates how strongly the material depolarizes light and ranges from 0 to 1 (Pasqual et al. 2015). In order to determine these values for the materials, they used a laser beam that they passed through several elements including a half wave plate and a quarter wave plate which allowed the laser's polarization to be controlled

(Pasqual et al. 2015).

Data was collected for six materials which include glossy white paint, matte black paint, black Kapton, Silver Teflon, aluminum alloy, and titanium alloy (Pasqual et al. 2015). They found that these materials did have “distinguishing polarimetric properties” that would allow debris to be identified by their polarimetric signature (Pasqual et al. 2015). Out of the properties being studied, the most applicable to the satellite research is the depolarization power. It was concluded that glossy white paint was a near perfect depolarizer, while all other materials were weak depolarizers (Pasqual et al. 2015).

A second area of research that was presented at the AMOS conference by Stryjewski et al. focused on creating accurate models that would describe the shape and material of a satellite. This is an important project because the reflected light polarization depends on the material, orientation, and shape of the satellite. Since the polarization is a result of all these factors it is difficult to be able to make conclusions about the orientation unless information about the shape is also known (Stryjewski et al. 2010). The fact that satellites are also composed of multiple materials only complicates the issue. Due to this, by modeling the shape and materials for a satellite it would then be possible to understand how the orientation might be changing.

This was accomplished by using computer software that has traditionally been used by computer game and movie animators who wanted to make images look as real as possible (Stryjewski et al. 2010). With these models, Stryjewski et al. were able to accurately describe the polarization state of light after it reflected off objects of varying shape and composition.

Several interesting results were found from this research. First, they found that the polarization signatures revealed additional information about the structure that was not contained by just looking at the intensity of light (Stryjewski et al. 2010). Second, they found that for simple shapes, the polarization signature was shape independent. For more complex shapes, this was not the case because the shape determined what materials were seen which changed the polarization signature

(Stryjewski et al. 2010). Ultimately, they concluded that with their model they can aid in identifying and monitoring satellites.

Finally, a third paper submitted to the AMOS conference explained the work done by Polo et al. focusing on characterizing geosynchronous satellites with polarimetry. They performed their work with two telescopes so that one could capture the polarized photometric measurements, while the other obtained non polarized measurements (Polo et al. 2016). Using the polarized data, they were able to construct the Stokes parameters that described how the light is polarized. The first parameter  $S_0$  is the total irradiance,  $S_1$  is the prevalence of horizontally polarized irradiance over vertically polarized irradiance, and  $S_2$  is the prevalence of linearly polarized irradiance at  $+45^\circ$  over linear polarized irradiance at  $-45^\circ$  (Polo et al. 2016). Using these parameters, they created light curves for four different geosynchronous satellites. They believed that the construction of these light curves was the first step in being able to characterize the satellites using polarimetry (Polo et al. 2016). They also noticed that there were differences in the curves for  $S_1$  and  $S_2$  that could hold useful information about the satellite (Polo et al. 2016). In the end they concluded that additional work was needed including observations of different satellite types and closer spaced measurements throughout the night to increase the resolution of the light curves (Polo et al. 2016).

## 1.4 Major Findings

At the conclusion of my research there were several major findings. First and foremost is the fact that light curves can be created for geosynchronous satellites using smaller, less expensive telescopes. These light curves are unique to the satellite and can be thought of as a satellite's signature. The signature itself depends on the orientation and composition of the satellite. Changes in the signatures are results of factors such as space aging, maneuvers, and the time of the year. It appears that with enough data and the results from other research it will be possible to classify

satellites based on their photometric signatures.

Another outcome is that some of the effects of space aging have been quantized for three geosynchronous satellites. These three satellites are AMC 15, DirecTV 8, and Spaceway 1. Data collected in the summer of 2018 was compared with data from the Geo Observations with Latitudinal Diversity Simultaneously (GOLDS) catalog which contained data from 2006 and 2011 for these satellites. For AMC 15 it was found that between 2011 and 2018 there was very little dimming, but there was a noticeable amount of reddening which was equal to about 0.1 magnitudes. Spaceway 1 did not show any signs of reddening, but it did appear about 0.1 to 0.2 magnitudes dimmer. However, DirecTV 8 showed neither signs of reddening nor dimming. Given these different results, it is clear that not all materials age the same way in space. It seems like the materials that AMC 15 and DirecTV 8 are composed of are more inclined to become redder, while those for Spaceway 1 are more prone to become dimmer with age.

Similarly, the polarimetric data for the satellites DirecTV 9s, SES 1, DirecTV 8, and DirecTV 4 contained information about the structure and movement of these satellites. Data were collected for the first three satellites on nine nights throughout the year. The first obvious result was that at different times of the year the polarized signatures change which seem to allow different structures on the satellite to be highlighted. During any given night, there is an ordering to how bright the satellite is in each of the four polarized filters. However, between when the December and May data were collected this ordering flips which is a feature that can be easily seen after the parameters  $S_1$  and  $S_2$  are calculated throughout the night. The last interesting feature was a sort of periodic oscillation or “ringing” that was seen in the  $S_1$  and  $S_2$  polarization fractions which may be connected to some sort of movement or flexing of the satellite throughout the night.

## 1.5 Overview

The remainder of the paper is organized in the following manner. Chapter 2 will begin with a brief explanation about some of the basics of the structure of geosynchronous satellites as well as some of the geometry of the sun, Earth, and satellite system. Afterwards, an overview of the options for studying geosynchronous satellites will be given as well as an explanation for why we chose certain methods. After these smaller discussions, the primary focus of the chapter will be presenting the methods for acquiring both the photometric and polarimetric data. In these sections, the procedures for gathering and processing the data will also be given.

Chapter 3 will then focus on analysis of the collected data. Photometric data will be presented first for AMC 15, DirecTV 8, and Spaceway 1 in order to take a look at the effects of space aging. Then the polarimetric data from three nights will be shown for DirecTV 9s, SES 1, and DirecTV 8 as well as the one night of data for DirecTV 4. Along with this data an analysis of the major features will be given.

Following these chapters, the appendix contains the remaining polarimetry data that was collected over the course of this research period. The appendix begins with the plots for DirecTV9, then SES 1, and finishes with the plots for DirecTV 8.

# Chapter 2

## Methods

### 2.1 Satellite System Geometry

The geometry of the satellite system plays a key role in the formation of the light curve signatures and must be considered when comparing data. This system is shown in Figure 2.1. The satellites orbit the Earth above the equator. When the satellites are highest or lowest they will have the same tilt as the Earth. This occurs either at the summer solstice when the satellites are seen with a  $+23.5^\circ$  tilt or at the winter solstice when they are seen with a  $-23.5^\circ$  tilt. Throughout the rest of the year the tilt will be at an intermediate value that varies sinusoidally.

Since there is a sinusoidal variation the tilt will be changing slowest near the solstices because the slope of the sine curve is small. Likewise, the greatest change will occur near the spring and fall equinoxes. Given this, signatures will be relatively stable around the solstice and more unstable at the equinoxes. So data taken near the solstice can be directly compared with data taken from a different year if it is also within a few days of the solstice.

A second aspect of the satellite geometry as shown in Figure 2.1 is that the solar panels are oriented in the North and South direction. This feature means that without any additional equipment

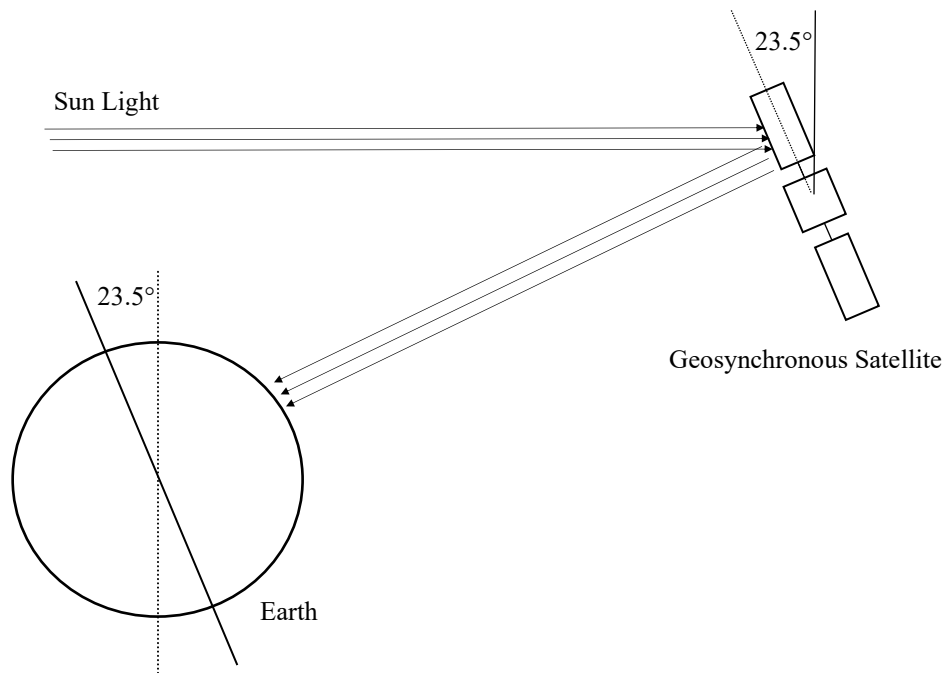


**Figure 2.1** Geometry of the Sun, satellite, and Earth system near the summer solstice. The tilt of the Earth is shown and the resulting tilt of the satellite.

the satellite has a basic North and South symmetry. Additional satellite communication structures will break this symmetry (Moody et al. 2018). Therefore, when looking at the signatures for these satellites they should be fairly symmetric. Any asymmetries in the signatures are caused by the additional structures.

## 2.2 Options for Studying Geosynchronous Satellites

While there is really only one way the photometry could be performed, there are two methods that can be used to collect polarized data. The first, as mentioned, is active polarimetry which is the method used by Pasqual et al. They preferred this method because it allowed them to capture more aspects of the polarimetric signature such as the diattenuation, retardance, and depolarization of the materials (Pasqual et al. 2015).

The second option is passive polarimetry, which is the method chosen for this research. Passive polarimetry uses the sun to illuminate the satellites and then examines the polarization of the reflected light. The sunlight is unpolarized, after it is reflected off the satellite any degree of polarization is caused by the satellite. By using the sun as the light source, passive polarimetry gives up some control. The primary draw for passive polarimetry is that it is a simpler setup. The main equipment that is needed is a telescope and Charge-Coupled Device (CCD) to take the images, as well as polarized filters. As will be shown in the analysis, there is still plenty to be learned from the polarimetry data obtained using passive polarimetry despite the simpler setup.

## **2.3 Photometric Methods Used**

Photometric data were collected using a 14-inch Celestron telescope at the ODIN laboratory located in Albuquerque, New Mexico. This telescope has a Software Bisque Paramount German Equatorial mount. The images were taken with a Finger Lakes Instrumentation (FLI) ML 16200 CCD with an FLI filter wheel in front of the camera. The satellites were observed using Johnson I, R, V, and B filters. This allowed us to find how bright a satellite was within a certain wavelength range of light. The telescope was controlled using Software Bisque Sky X Professional Edition.

Our goal was to obtain as much data on these satellites as possible. We wanted to collect data on a number of satellites throughout the year. This would allow us to have a signature for the satellite at any given time of year. Table 2.1 shows a complete list of all of the satellites that have currently been observed, as well as the date and type of observations that have been taken. Polarimetric observations began in 2017 and continued until the summer of 2018 while photometric data was only collected during the summer. All of the satellites except DirecTV 4 have at least one night of photometric data from the summer of 2018. Since they only have one or two nights of data, there still is a need for further data collection. This need is further emphasized by the fact that

polarimetric data has only been obtained for four satellites.

**Table 2.1** A comprehensive list of the geosynchronous satellites that have been observed. The satellite is listed with the day it was observed as well as whether it was observed using polarimetry, photometry.

Satellite	Date Observed	Observation Type
AMC 15	June 19 2018	photometric
DirecTV 4	Sept 26 2017	photometric
DirecTV 8	Oct 28 2017	polarimetric
	Dec 18 2017	polarimetric
	Feb 7 2018	polarimetric
	Feb 16 2018	polarimetric
	April 9 2018	polarimetric
	May 3 2018	polarimetric
	May 25 2018	polarimetric
	June 4 2018	photometric
	June 7 2018	polarimetric
June 18 2018	photometric	
DirecTV 9s	Sep 26 2017	polarimetric
	Oct 28 2017	polarimetric
	Dec 18 2017	polarimetric
	Feb 7 2018	polarimetric
	Feb 16 2018	polarimetric
	April 9 2018	polarimetric
	May 3 2018	polarimetric
	May 25 2018	polarimetric
	June 4 2018	photometric
June 7 2018	polarimetric	
June 18 2018	photometric	
DirecTV 10	June 20 2018	photometric
DirecTV 12	June 20 2018	photometric
DirecTV 15	June 20 2018	photometric
SES 1	Sep 26 2017	polarimetric
	Oct 28 2018	polarimetric

---

	Dec 18 2017	polarimetric
	Feb 7 2018	polarimetric
	Feb 16 2018	polarimetric
	April 9 2018	polarimetric
	May 3 2018	polarimetric
	May 25 2018	polarimetric
	June 4 2018	photometric
	June 7 2018	polarimetric
	June 18 2018	photometric
SES 3	June 20 2018	photometric
SES 11	June 19 2018	photometric
Spaceway 11	June 20 2018	photometric

---

Within any given night there was a set procedure that had to be followed in order to obtain useful data. For data to be useful we needed to have the highest signal-to-noise ratio possible. The signal is determined by the brightness of the object being looked at and is recorded by the CCD. A CCD is an array of pixels that counts the number of photons from the object hitting it per pixel per second. So a brighter object would have a higher photon count than a dimmer one. Noise, on the other hand, is defined as photons counts recorded by the CCD that do not come from the object.

As part of the telescope setup the CCD had to be cooled to about  $-20^{\circ}\text{C}$ . The purpose of this is to reduce any thermal noise in the data being collected. At a higher temperature, currents can exist within the CCD which will increase the recorded counts. However, by keeping the CCD cooled most of these currents, known as dark currents, can be eliminated.

With the telescope set up and the CCD cooled, the next step was to take calibration frames. These frames are meant to further account for noise and remove it from the actual satellite data. There are three types of calibration frames that need to be taken. The first is called biases or zeroes. This is a zero second exposure with the camera shutter closed. These frames are meant to correct for an artificially induced electronic offset, which ensures that the Analog-to-Digital Converter always receives a positive signal, and correct for any read noise. Simply put, without any light present

each pixel has a small number of counts given to it so that a negative signal can never be measured. Between 25 and 30 bias frames are taken, stacked, normalized, and are subtracted from the other frames to remove this offset.

The second type of calibration frames taken are called darks. These frames are taken with the camera shutter closed for the same length of time as the exposures for the satellites being observed that night. The purpose of darks is to remove the counts that come from the dark current. It is necessary to take them for the same amount of time as the satellite exposures because it allows the total average dark current to be taken into account. In a standard night, approximately seven to ten darks are taken for each exposure length. The darks are then stacked by exposure time, normalized and subtracted from the remaining frames.

Finally, the third type of calibration frames are flat fields. Not all of the pixels within the CCD respond to light the same way. Within a CCD there are pixels that are more or less sensitive to the same amount of light. Flat fields are used to correct for this as much as possible as well as any vignetting from the optical system. To take a flat field the telescope is pointed at a portion of the sky that is uniformly illuminated within the field of view of the CCD. The sky is most uniformly bright shortly after sunset with the telescope pointed a few degrees East of directly overhead. The flats are taken in each filter that is being used because the pixels will also respond differently to different wavelengths of light. The flats are then combined within each filter and divided out from the satellite images.

The process of subtracting zeroes, darks, and flats is known as data reduction. There are several software packages that are able to automatically perform these tasks. The most commonly used software within astronomy is IRAF. However, for this research the photometric data was reduced using the tools in AstroImageJ because it was a free software package that could accurately perform the necessary reduction.

After taking these calibration frames we began taking science frames of the satellites we were

studying that night. As mentioned, we observed the satellites using the Johnson B, V, R, and I filters. Using the Sky X we set up exposure series which would take approximately 3 exposures in a particular filter before rotating to the next filter. Exposure times were chosen so that there was a good enough difference in counts between the satellite and the sky. Generally, exposures were between 10 and 15 seconds with some variation between filters since the satellites are not equally bright in all filters. After collecting as much data as possible in a night, these frames were reduced by applying the zeroes, darks, and flats.

We then performed aperture photometry using AstroImageJ to determine the total counts per pixel coming from the satellites. The process of aperture photometry begins by placing a circle around the satellite in the frame. Then all of the counts within this circle are summed up. This value will represent the number of photons coming from the satellite and the sky. It is necessary to choose the appropriate aperture size so that all the light from the satellite is accounted while minimizing the background light from the sky because otherwise there would be additional errors in the calculations. A second aperture is then placed around the first, which sums up all of the counts per pixel that come from only the sky. This value is then subtracted from the value for the inner aperture and the result is the counts per pixel for just the satellite.

The value for the counts per pixel is then divided by the exposure time in order to calculate the counts per second per pixel. It is this value that can then be used to calculate the satellite brightness using the standard magnitude scale. The apparent satellite magnitude is found using the equation  $m = -2.5 \log_{10}(\text{counts/sec}) + C$ . To find the uncalibrated magnitude the constant  $C$  can be ignored, but to calibrate the magnitude the value for  $C$  must also be calculated.

The constant is affected by both the time of night and the filter being used. This is because atmospheric variations will change how bright the satellite appears and this will not be uniform in all the wavelengths of light. So to determine the constant, we observed standard fields of stars throughout the night. These star fields contain stars with accepted magnitudes that are not noticeably

variable. The magnitudes for these stars and their specific star field are published in the Landolt Standard Fields Catalog. About every hour or two, we observed the nearest standard field in the filters being used. We then employed the same photometric process to determine the uncalibrated magnitudes for several of the stars in the field. The difference between these magnitudes and the published ones represent the value of  $C$  at that time of the night. We calculated the  $C$  value each time a standard field was observed and found the best fit equation which would describe how  $C$  varied throughout the night in each filter. With this equation it was then possible to calibrate the satellite B, V, R, and I magnitudes.

With the data processed and calibrated, it was then possible to plot the magnitude versus the time of night to create light curves for the satellites. Using a MATLAB script, written by Steve Gregory, the time of night was converted into solar phase angle. The result was a light curve that showed how the brightness of a satellite in a specific filter changed as a function of phase angle. These light curves became the signatures for the satellites.

Light curves were also created from the photometric data contained in the GOLDS catalog. The catalog contained magnitudes for some of the satellites from 2006 and 2011. By using this data, we were able to see how the signature of the satellite changed over time due to space aging. It was important to find data from the same time of year because, as mentioned, the signature changes throughout the year. Fortunately, because we were near the summer solstice, we could compare data from different years that was taken within about a week of the day we took our data.

Since we had light curves for the satellites in different filters, it was also possible to calculate the B-V color for the satellites as a function of phase angle. This is done by subtracting the V magnitude from the B magnitude. A redder object will be brighter in the V filter than in the B filter. Since the magnitude scale is reversed where a higher magnitude represents a dimmer object, a redder object will have more negative V magnitude and thus a more positive B-V color. By calculating the color for these satellites and comparing it to the GOLDS data we were able to see how the color changed

as a result of space aging.

## 2.4 Polarimetric Methods Used

Polarimetric data were collected using the 16-inch telescope at the Remote Observatory for Variable Object Research (ROVOR) located in Delta, Utah. Polarimetric and photometric data were acquired essentially the same way. However, instead of using the B, V, R, and I filters, we inserted four plane-polarized filters into the filter wheel. These filters were oriented at  $0^\circ$ ,  $45^\circ$ ,  $90^\circ$ , and  $135^\circ$ . With the degrees being measured from the north and south direction and rotating counterclockwise. We also combined these filters with a V filter to look at only the visible light range.

Data frames were collected using these four filters and was reduced using the same processes outlined previously. Aperture photometry was also performed in the same manner to find the counts coming from the satellites in each of the polarized filters. The counts again relate to the photons received at the CCD, but because they have passed through the polarized filters they are the number of photons with the same polarization angle as the filters. Since we had the counts per second, after performing the aperture photometry, we defined the counts as the flux from the satellite in a given polarization angle. These fluxes will be designated as  $F_0$ ,  $F_{45}$ ,  $F_{90}$ ,  $F_{135}$  and will be used when calculating the Stokes Parameters that can describe how light is polarized.

Before calculating the parameters for the satellites, a several step calibration process had to be completed once for the telescope and filters. This process was performed previously for the ROVOR telescope and was performed at the end of the summer of 2018 for the ODIN telescope. The calibration method is detailed in a technical report by Moody et al. as well as a currently unpublished paper by Moody, but it will be summarized here.

The first step of calibrating the polarized filter is to observe polarimetric standard stars. According to Moody these stars have been calibrated for general use by the Subaru FOCAS team and

contain a list of polarized and unpolarized stars known as Serkowski standards (Moody et al. 2018). The polarized and the unpolarized stars each help with a different calibration piece and both need to be observed.

The unpolarized standards are used to calibrate the throughputs of each filter (Moody et al. 2018). Since the Stokes parameters depend on the amount of flux through one polarization orientation versus another it is important that each polarized filter allows the same amount of light through for an unpolarized source. Figure 2.2 taken from Figure 4 of Moody (2018) shows the results of observing five unpolarized standard stars using the ROVOR telescope. The data points were normalized by dividing the counts in each of the polarization filters by the mean counts of all four of the filters. From the figure it is clear that the normalized values are centered around 1 for the different stars. This means that the throughput for the ROVOR filters is about the same in each filter and no additional adjustments need to be made (Moody et al. 2018).

The polarized stars were observed to correct for the effects of filter misalignments. Since the filters were put in the filter wheel by hand, there may be small misalignments in their angles. To calculate this error, the orientation of the polarization ellipse was calculated using the fluxes in each filter according to the method in Moody (2018). This calculated orientation was then compared to the published value given by the Subaru FOCUS team. By plotting the published values versus the calculated values for all the polarized stars observed, it was then possible to determine a linear relationship between calculated and true polarization angles (Moody et al. 2018). For the ROVOR telescope this relationship ended up being that  $\text{True Angle} = 0.9929(\text{Calculated Angle}) - 4.2957$ . Since the multiplier 0.9929 is close to 1 it means that there is a good linear result between the calculated and true angle. The -4.2957 means that the alignment with north is about 4° clockwise to the north (Moody et al. 2018). This relationship can then be applied to all calculation to find the true polarization angle for the satellites.

The polarization of light is typically represented as an ellipse giving the integrated strength

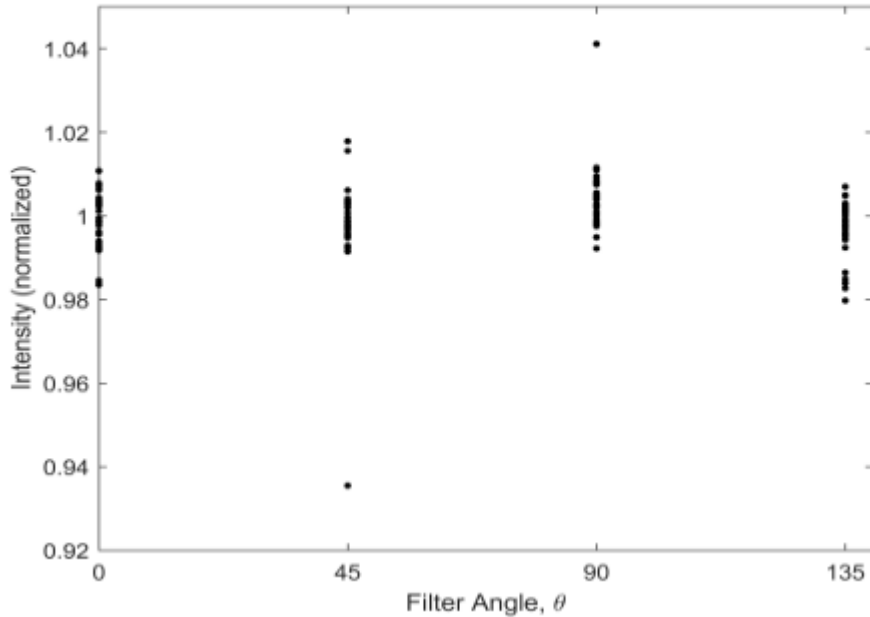


**Figure 2.2** Taken from Moody (2018). This is the normalized data for 5 unpolarized standard stars observed with the ROVOR telescope. The data points were normalized by dividing the counts in each filter by the mean counts in all four filters. Since the values are centered around 1 the throughput from each filter can be taken as being the same.

of the electric vector in an x-y plane. This ellipse is shown in Figure 2.3 which was taken from Moody et al. The angle  $\theta$  is the polarization angle and is measured from the x axis. The value  $a$  is the semimajor axis of the ellipse and  $b$  is the semi-minor axis. The percentage of polarization is given by the ratio  $b/a$  and is equal to 0 for completely polarized light and 1 for unpolarized light (Moody et al. 2018). A polarization state can be described using four characteristics which are: the ellipticity of the polarization ellipse, the orientation of the ellipse, the chirality (handedness) of the ellipse, and the degree of polarization (Moody et al. 2018).

These polarization characteristics are found by calculating the Stokes parameters. The first parameter is  $S_0$ , which is the flux density of unobstructed light. This is only necessary to calculate

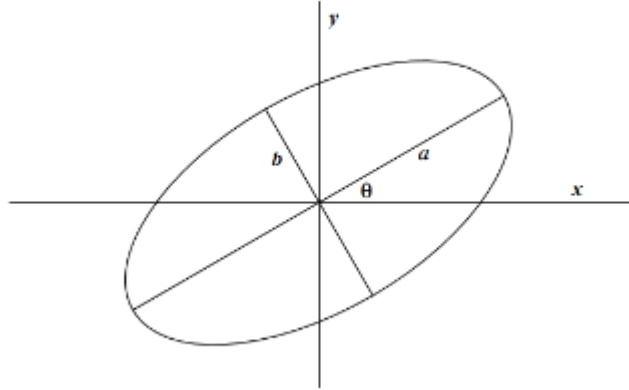


**Figure 2.3** Taken from Moody (2018). This shows the polarization ellipse for light coming out of the page. The angle  $\theta$  is the polarization angle which is measured counterclockwise from the x axis. The values  $a$  and  $b$  represent the semimajor and semi-minor axes

when absolute calibration is needed. For this research absolute calibration is not needed (Moody et al. 2018). This value can then be set to 1. The other two parameters of interest are  $S_1$  and  $S_2$ . As mentioned in Chapter 1,  $S_1$  is the prevalence of horizontally polarized irradiance over vertically polarized irradiance, and  $S_2$  is the prevalence of linearly polarized irradiance at  $+45^\circ$  over linear polarized irradiance at  $-45^\circ$  (Polo et al. 2016). The equations for these parameters are as follows:

$$S_1 = \frac{2(F_0 - F_{90})}{(F_0 + F_{45} + F_{90} + F_{135})} \quad (2.1)$$

$$S_2 = \frac{2(F_{45} - F_{135})}{(F_0 + F_{45} + F_{90} + F_{135})} \quad (2.2)$$

Using these two parameters the ellipticity  $e$  and the polarization angle  $\theta$  can be calculated using the following known relations. They are:

$$e^2 = \frac{2\sqrt{S_1^2 + S_2^2}}{1 + \sqrt{S_1^2 + S_2^2}} \quad (2.3)$$

$$\theta = \frac{1}{2} \arctan \frac{S_1}{S_2} \quad (2.4)$$

These equations were used with the polarimetric data that were collected on the various nights of the year so that the parameters  $S_1$ ,  $S_2$ ,  $\theta$ , and  $e$  could be found as a function of solar phase angle. After each cycle of going through the polarization filters, the four fluxes could be calculated. The Stokes parameters, ellipticity and the polarization angle were then found at each point in the night. Using the same program in MATLAB, written by Steve Gregory, which turned the observation time into phase angle, we were able to plot these calculated values against the phase angle. This left us with three plots per night and per satellite. We had one plot of the four fluxes, one that shows the polarization fractions  $S_1$  and  $S_2$ , and the last shows both the ellipticity and polarization angle. These plots allowed me to characterize the curves with the intent of being able to understand the satellite structure and movements throughout the night or year.

# Chapter 3

## Results and Conclusions

Our goal was to use our photometric data to create light curves that could become a signature for the satellites and indicate the signs of space aging. In addition, we created polarized light curves and calculated the Stokes parameters to begin to analyze how the polarized light allows us to understand the structure of the satellite and any maneuvers it makes. The first section of this chapter will address the results related to space aging. The subsequent sections will then focus on characterizing the polarized data for the satellites. My final conclusions will then be presented.

### 3.1 Photometric Evidence of Space Aging

Using the data collected, we constructed light curves and color plots for all of the satellites observed. However, the GOLDS catalog did not contain data for all of these satellites within a small enough day-of-the-year window. Without this data, it was not possible to look at the effects of aging. So the light curves for these satellites will not be presented here. Instead light curves and the color plots are shown for AMC 15, DirecTV 8, and Spaceway 1. From these plots, we found that—depending on the satellite—the effects of aging were shown by either reddening or by dimming, but the effects were not the same between satellites.

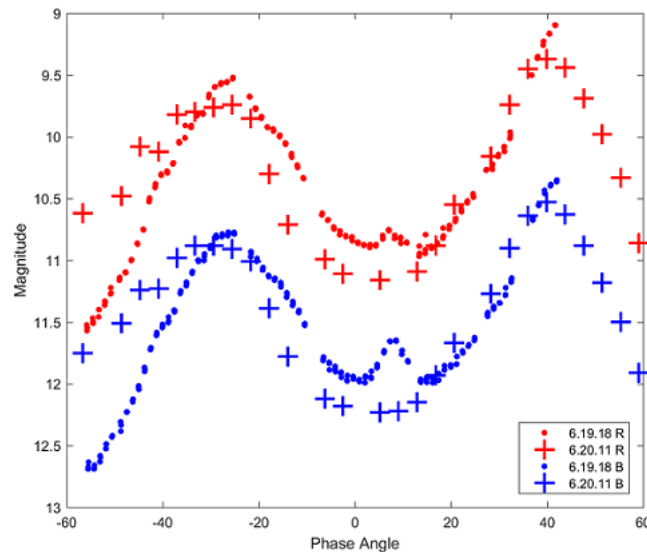


**Figure 3.1** B (blue) and R (red) magnitudes for AMC 15 from 2018 (dots) compared to data taken in 2011 (+) from the GOLDS catalog. The apparent magnitudes change as a function of solar phase angle. The overall shape and amplitude of the light curves has stayed essentially the same within the seven-year observation gap; no signs of dimming are evident. The signatures appears to be slightly shifted in the 2018 data. The minor peak at  $8^\circ$  phase angle is most likely a result of an adjustment with the solar panels.

In Figure 3.1 the B and V magnitudes from 2018 plotted against the phase angle for AMC 15 are compared to the data from the GOLDS catalog. The first important feature is that within the seven year gap between observations, the signature for AMC 15 stayed essentially the same. However, there are a couple of slight changes that have occurred. First, the entire signature has shifted slightly to the right. This shift makes it look like the satellite is dimmer when phase angle is  $-60^\circ$  to  $-30^\circ$  and then appear brighter when phase angle is  $-30^\circ$  to  $-10^\circ$ . Once this shift is taken into account, however, the brightness throughout the night is essentially the same between the two sets of data. A small peak occurs at approximately  $8^\circ$  phase angle in the 2018 data that is not found in the 2011 data. This difference is most likely a result of a maneuver or an adjustment of the solar panels.

Another look at AMC 15 is provided by the B-V color graph shown in Figure 3.2. A noticeable

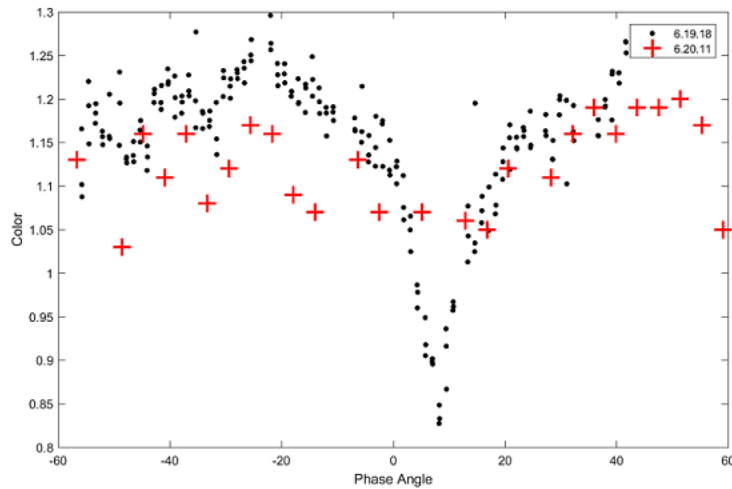


**Figure 3.2** B-V color for AMC 15 from data taken in 2018 (dots) compared to data from the GOLDs catalog taken in 2011 (+). For most of the night in 2018 AMC 15 has a higher color index than the GOLDs data by approximately 0.1. Over the period of seven years, AMC 15 has become redder due to space aging. The drop in color near  $8^\circ$  phase angle is linked to the peak seen at the same time in Figure 3.1 and supports the claim that light is being scattered off a solar panel.

trend is evident despite a bit of scatter in the color measurements. For most of the night, the 2018 data has a greater B-V color than the GOLDs data. On average AMC 15's color is approximately 0.1 greater than the 2011 data. As explained in Sec 2.3, a higher color index indicates a redder object. Thus, within the seven year observation gap, AMC 15 has become redder due to space aging. The one exception occurs in the region around  $8^\circ$  phase angle. In this region, AMC 15 appears to be much bluer than it was in 2011. This region coincides with where the new peak is located in Figure 3.1. The bluer scattered light from AMC 15 at this point again supports the claim that the light coming off a solar panel is being seen and causing the satellite to appear bluer during this time.

Similar to AMC 15, DirecTV 8 did not show any clear signs of dimming from its light curve. The B and R light curves are shown in Figure 3.3. Again the data from 2018 is shown with the data from the GOLDs catalog, which was taken in 2006 in this case. The GOLDs data ends near  $20^\circ$  phase angle, so the two data sets cannot be compared for the entire night. However, where both data

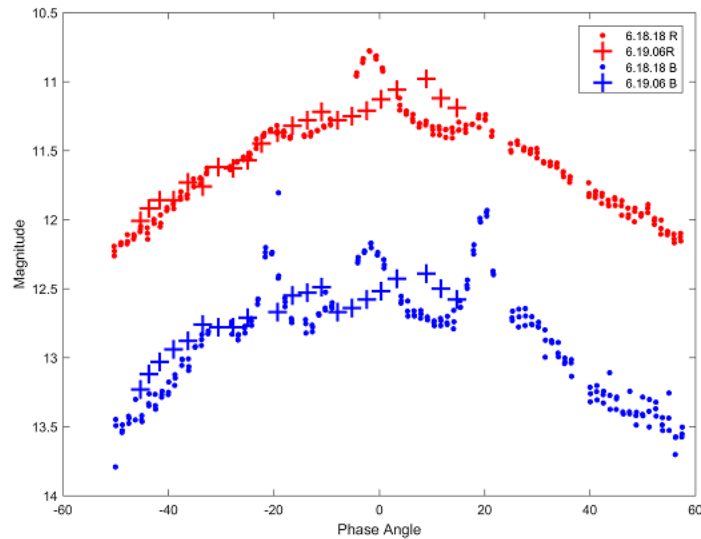


**Figure 3.3** B (blue) and R (red) magnitudes for DirecTV 8 plotted against phase angle from data taken in 2018 (dots) compared to data from the GOLDs catalog taken in 2006 (+). The overall shape and amplitude of the curves stayed essentially consistent over the 12 year observation gap. This suggests no dimming as a result of space aging. However, the two new peaks located at  $\pm 20^\circ$  phase angle likely are the result of solar panels being adjusted at some point within the observation gap.

sets exist it is possible to compare the signatures for DirecTV 8. By comparing the data, it is clear that there has been very little change over the years. Specifically, for the first half of the night in the R filter, the two light curves are essentially the same. This result indicates that DirecTV 8 has not become dimmer due to space aging. A difference in the signatures is evident in the B filter where the 2018 data now has two side peaks located at  $\pm 20^\circ$ . Like the peak that showed up in the 2018 data for AMC 15, these peaks are most likely a result of adjustments made to the solar panels.

Not only does DirecTV 8 not show signs of dimming, it shows no signs of becoming redder over the 12 years between observations. Figure 3.4 shows the B-V color for DirecTV 8 as a function of phase angle along with the calculated color from the GOLDs data. Again it is difficult to draw absolute conclusions because of the lack of data from the GOLDs catalog. However, where there is GOLDs data it seems to be in pretty good agreement with the calculated color from the 2018 data.

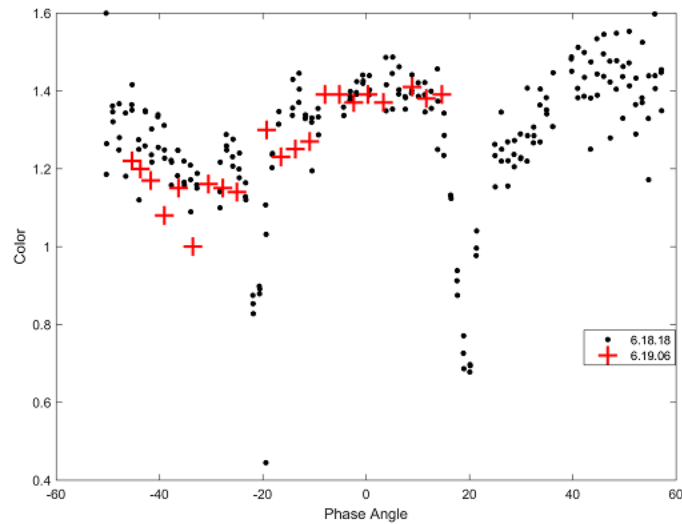


**Figure 3.4** B-V color versus phase angle for DirecTV 8 data taken in 2018 (dots) compared to data from the GOLDS catalog taken in 2006 (+). For the first half of the night, where there is data from the GOLDS catalog, there are no signs of reddening since the both data sets overlap each other. There is a drop in the color index at  $\pm 20^\circ$  phase angle in the 2018 data. Since this drop lines up with the new peaks in the B filter light curve it reinforces the theory that the new peaks are caused by solar panels being adjusted and allowing more blue light to be seen.

Since there is essentially no change in the color between 2006 and 2018, it is clear that DirecTV has not become redder. The 2018 data does show a drop in the color index at  $\pm 20^\circ$  phase angle which, is at the same location as the new peaks in Figure 3.3. This drop supports the theory that the solar panels have been adjusted since light coming off of a solar panel will be bluer.

Since each satellite seems to age differently, it is necessary to look at each satellite individually. Figure 3.5 shows B and R magnitudes for Spaceway 1 plotted against the phase angle. The data collected in 2018 is displayed with data from 2011 which was obtained from the GOLDS catalog. Two interesting features can be seen from the figure. The first is that over the seven years between the observations, the signature has remained essentially the same shape wise. The second is that the 2018 data is about 0.1 to 0.2 magnitudes higher throughout the night: In the seven years, Spaceway 1 has become about 0.1 to 0.2 magnitudes dimmer since a higher magnitude corresponds to a dimmer

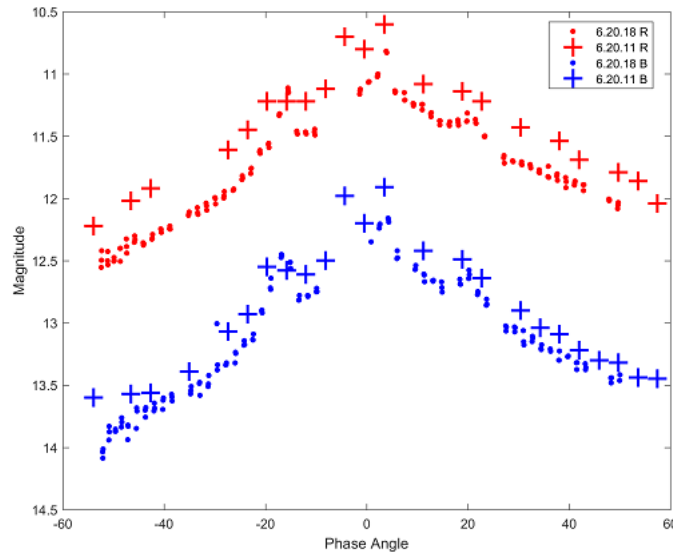


**Figure 3.5** B (blue) and R (red) magnitudes for Spaceway 1 (dots) compared to data from 2011 (+) obtained from the GOLDs catalog. Showing how the satellite brightness changes in B and R filters with phase angle. The signature has remained essentially the same, but increased by approximately 0.1 to 0.2 magnitudes: This means over in the seven year gap between measurements Spaceway 1 has become dimmer since a higher magnitude corresponds to a dimmer object.

object. While this may not seem like a major change, since the magnitude scale is logarithmic a 0.1 drop in magnitude indicates a large drop in brightness.

While it is clear that Spaceway 1 has become dimmer over time due to space aging the trend is less clear in its color. Figure 3.6 shows the color for Spaceway 1 calculated from data taken in 2018 compared to the color calculated from GOLDs data taken in 2011. There is sizeable scatter in the color for Spaceway 1 throughout the night for both data sets. However, in the GOLDs data there does appear to be a loose downward trend for the beginning of the night and an upward trend for the second half of the night. Despite the scatter in the 2018 data, the same general color trend can be seen as in the GOLDs. Ultimately, there is no evidence suggesting that Spaceway 1 has become redder over time due to space aging based on this data.

The analyses of these satellite light curves indicate nonuniform effects of space aging. AMC 15

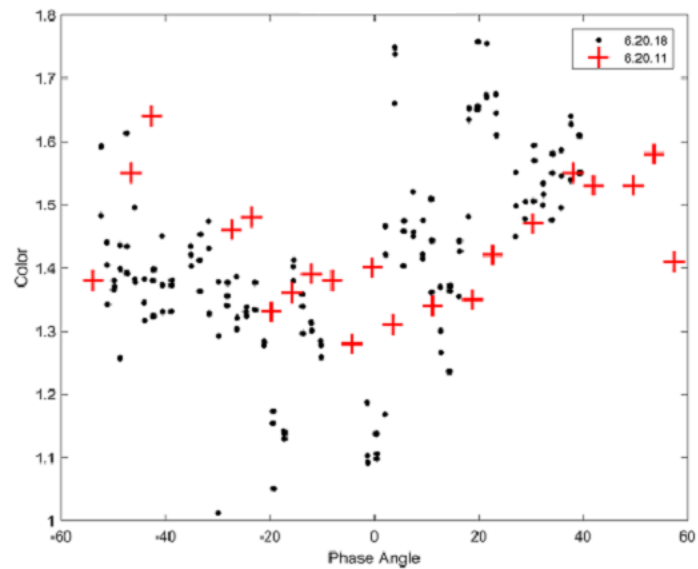


**Figure 3.6** B-V color for Spaceway 1 using data from 2018 (dots) compared to data from the GOLDs catalog (+). Both data sets have a fair amount of scatter with a bit clearer trend appearing in the GOLDs data. Based on the scattering in the color values, there are no obvious signs of reddening due to space aging.

showed clear signs of reddening, Spaceway 1 showed signs of dimming, and DirecTV 8 did not show signs of either. However, the results do support the theory that the effects of space aging are manifested by both reddening and by dimming. The difference in aging is most likely a result of composition. Different materials are going to age in different ways at various rates. Thus, materials used to create a certain satellite will define how the satellite ages in space.

Additional insight can be gleaned from differences between light curves for each satellite. Each satellite's curve has unique features which allow them to be distinguished from each other. This difference supports the philosophy that the light curves can be used as signatures to identify the satellites. When two signatures taken at the same time of year for the same satellite are compared the differences are a result of maneuvers and adjustments made to the satellite.

## 3.2 Key Features in Polarimetric Data

In this section, the data for the four satellites observed using polarized filters will be presented. This data is meant to help gain an understanding of how the satellite structure and any movements will affect how the light is polarized. For each night, plots of the flux in each filter, the Stokes parameters  $S_1$  and  $S_2$  polarization fractions, and the position angle as well as the eccentricity are shown. With the exception of DirecTV 4, which was only observed once, these satellites were observed between nine and ten times in polarized filters. Three nights of data for each satellite are presented to show key features in their signatures as well as in the polarization parameters. The remaining data can be found in the appendix which is divided into sections for each satellite.

### 3.2.1 Polarimetry of DirecTV 9S

The results of the polarimetry data for DirecTV 9S are presented in Figure 3.7. To characterize this data, it is first useful to look at the light curves which show the flux measured in the four

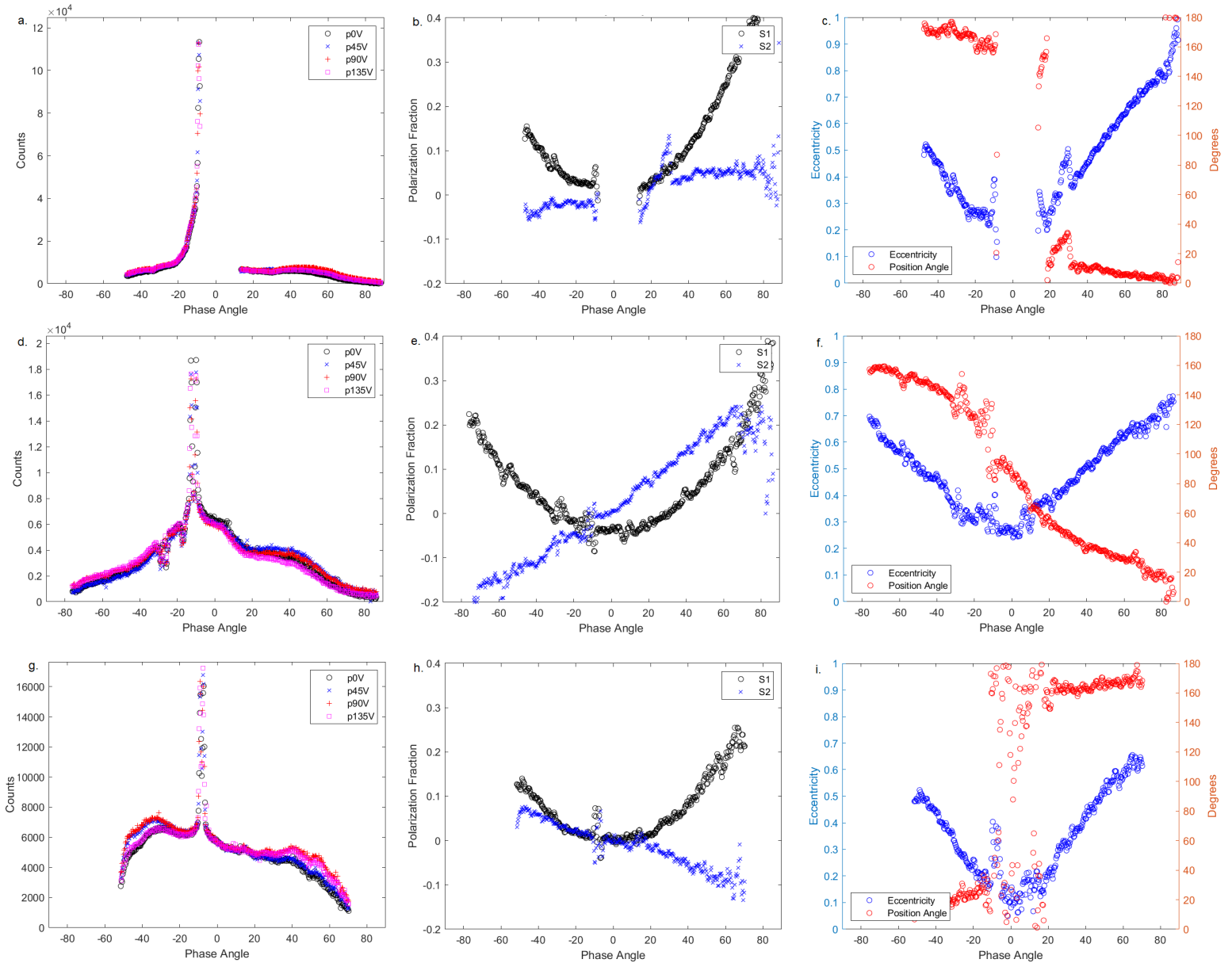


**Figure 3.7** Polarimetric data for DirecTV 9S. Each plot shows values plotted against the phase angle. Plots (a)-(c) are for data taken in September, (d)-(f) are for December, and (g)-(i) are for May. Plots a,d,and g show the flux in each of the four polarized filters; (b),(e), and (h) are the calculated Stokes parameters  $S_1$  and  $S_2$ ; and (c),(f), and (i) show the position angle as well as eccentricity. It is interesting to see the variation in the flux signatures between nights, while the  $S_1$  and  $S_2$  polarization fraction trends have little variation. Also noteworthy is the change in slope of the  $S_2$  polarization fraction between Plots e and h.

polarized filters. Figures 3.7(a), 3.7(d), and 3.7(g) show these curves for data collected in September, December, and May respectively. Two main features stand out in these plots. The first is that the signatures vary greatly throughout the year. For example, the September data is dominated by a single peak whereas in December, there is a much smaller peak and some additional features on the side like the two drops in flux occurring at  $-28^\circ$  and  $-18^\circ$  phase angle. The second key feature is how the flux ordering changes throughout the year. For the second half of the night in September and December the fluxes are ordered such that  $F_{45} > F_{90} > F_0 > F_{135}$ . However in May this changes so that  $F_{90} > F_{135} > F_{45} > F_0$ . This change is most likely due to the viewing angle changing from negative to positive after the spring equinox

While the light curves themselves vary greatly throughout the year, the  $S_1$  and  $S_2$  polarization fractions shown in Figures 3.7(b), 3.7(e), and 3.7(h) stay much more consistent. Each night  $S_1$  varies parabolically, while  $S_2$  increases linearly. Again there are two areas to note. The first is the spike in the  $S_2$  polarization fraction occurring at  $+30^\circ$  phase angle in Figure 3.7(b). This spike is interesting because there is not a corresponding feature in the light curve in Figure 3.7(a). Clearly the light at this point is being polarized due to a reflection off a particular piece of the satellite. However, because the central peak of Figure 3.7(a) dominates so heavily, there is not a visible corresponding feature. The second noteworthy feature is how the  $S_2$  polarization trend changes so that it has a negative slope in Figure 3.7(h). This change is caused by how the flux orderings change throughout the year and therefore is most likely due to the viewing angle.

Similar to the polarization, the eccentricity and position angle trends throughout the night—seen in Figures 3.7(c), 3.7(f), and 3.7(i)—stay very consistent between nights. Generally, the eccentricity decreases linearly for the first half of the night and then increases for the second. As can be seen, the minimum eccentricity occurs each night near  $0^\circ$  phase angle which means at this point the light coming from the satellite is the least polarized. In Figure 3.7(c), there is also a spike in the eccentricity occurring near  $+30^\circ$  phase angle which is connected to the same spike in the

$S_2$  polarization fraction mentioned earlier. It seems as though all the calculated values exhibit a flip between the December and May data. So this flip is also seen with the changing trend for the position angle between Figure 3.7(f) and Figure 3.7(i).

Throughout the year, the light curves for DirecTV 9S vary to a large degree. These variations are likely a result of the angle at which the satellites are seen. Unlike the fluxes in each filter, the polarization fractions do not seem to change nearly as much. Given this stability, the polarization fractions may be used as a secondary and more constant signature for these satellites. The polarization fraction also seems to contain information that is not readily seen in the light curves themselves, such as the case seen in Figures 3.7(a) and 3.7(b).

### 3.2.2 Polarimetry of SES 1

The polarimetry data for SES 1 shows similar trends seen in the data for DirecTV 9S. The SES 1 data from September, December, and May is shown in Figure 3.8. The changing flux signatures are shown in Figures 3.8(a), 3.8(e), and 3.8(g). In the September data, shown in Figure 3.8(a), there is a broad peak centered at  $-23^\circ$  phase angle and a smaller peak that occurs at  $+37^\circ$  phase angle. This second peak is likely the result of light being reflected off a structure on the side of the satellite. Then, as seen in Figure 3.8(e), the signature changes so that it is now dominated by a single peak that has a small drop in flux occurring right before the peak. While the signature does change dramatically throughout the year, it is also noteworthy to see how the signatures in September and May [Figures 3.8(a) and 3.8(g)] have essentially the same shape.

While still being unique, the  $S_1$  and  $S_2$  polarization fraction [seen in Figures 3.8(b), 3.8(e), and 3.8(h)] do resemble those found for DirecTV 9S. Once again the  $S_1$  polarization fraction varies parabolically and the  $S_2$  fraction varies linearly. Also similar to DirecTV 9S, there is the same flip in the slope for the  $S_2$  polarization trend which occurs between the December and the May data. The most interesting  $S_1$  and  $S_2$  signature is the one for the December data seen in Figure 3.8(e).

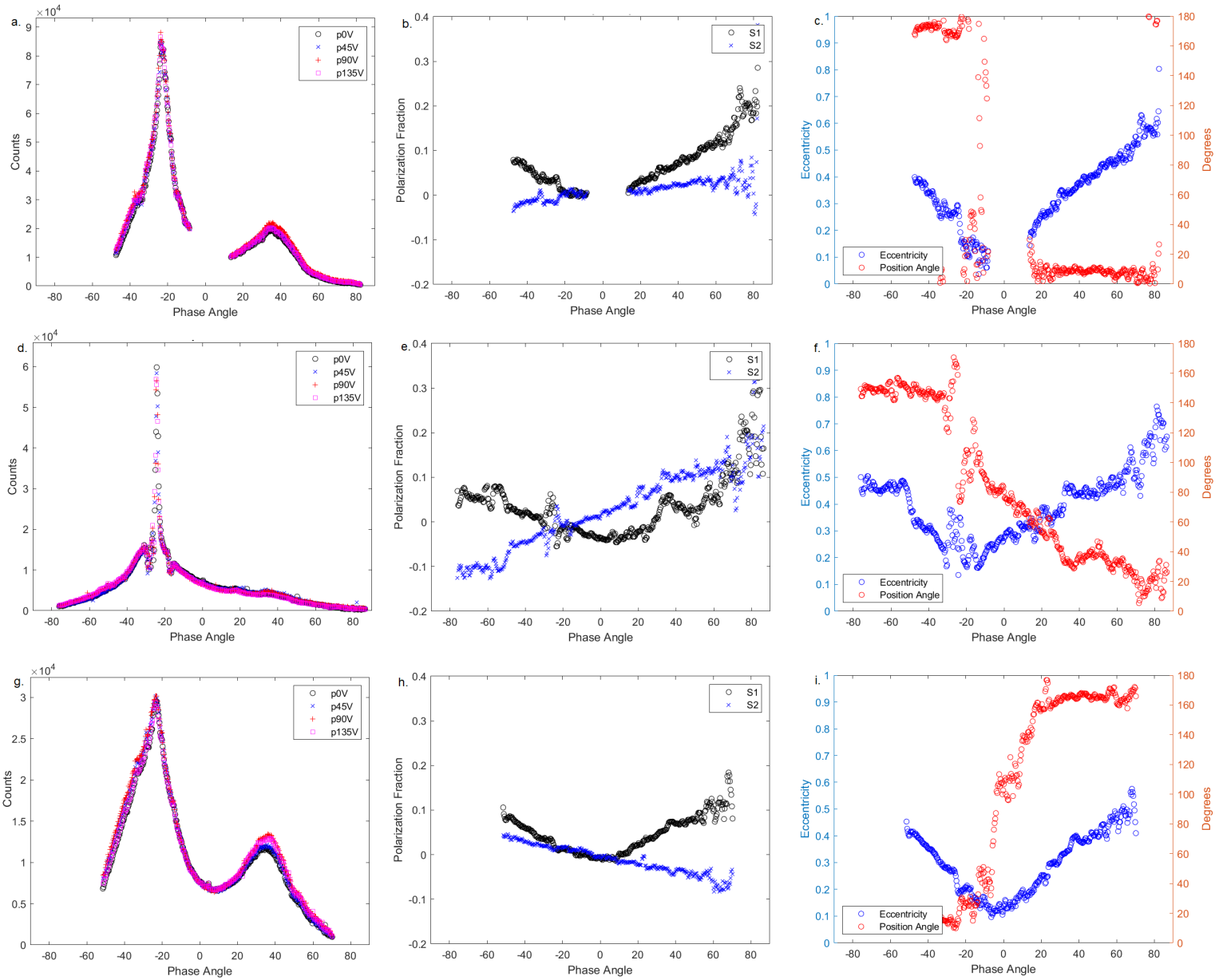


**Figure 3.8** Polarimetric data for SES 1. Each plot shows values plotted against the phase angle. Plots (a)-(c) are for data taken in September, (d)-(f) are for December, and (g)-(i) are for May. Plots (a),(d),and (g) show the flux in each of the four polarized filters; (b),(e), and (h) are the calculated Stokes parameters  $S_1$  and  $S_2$ ; and (c),(f), and (i) show the position angle as well as eccentricity. From Plots (a),(e),and (g) it is seen that the signature changes throughout the year but then returns to its original shape. There is also a sort of ringing in the polarization fractions shown in Plot (e) which should be connected to movements made by the satellite.

This signature is worth taking a closer look at for two reasons. The first is that while the flux plot for this night shows very few features, the polarization fractions show many small spikes where the polarization increases. Therefore, there is additional information contained in the polarization signature that is not easily observed by only looking at the flux plot. The second major feature seen in the signatures is a small periodic variation or “ringing” in both polarization fractions. Currently, the exact cause of the ringing is unknown. Still, it is also interesting to see that in the beginning of the night the  $S_1$  and  $S_2$  ringing is in opposite directions, while in the second half of the night it is in the same direction.

Again, like DirecTV 9S, the eccentricity as a function of phase angle shown in Figures 3.8(c), 3.8(f), and 3.8(i) is essentially v-shaped. The minimum eccentricity always occurs at the same time as the major peak in the plot for the flux. This means that when the satellite is seen directly face on, the light is the least polarized. The eccentricity plots also show some of the same variations that can be seen in the  $S_1$  and  $S_2$  plots indicating that the light is being polarized more or less by pieces of the satellite at certain times throughout the night. The position angle for the first two nights drops from being between  $160^\circ$ - $180^\circ$  to being between  $0^\circ$ - $20^\circ$ . However, this trend again flips in May which should again be a result of the changing viewing angle.

A comparison of the results from the polarimetry data for DirecTV 9s and SES 1 shows several similarities and differences. Importantly, the signatures created from either the flux or the Stokes parameters are completely different between the satellites. This means that whether standard photometric or polarized filters are used, the resulting light curves can be used to identify the satellite. The fact that the slope of  $S_2$  changes in the May data for both satellites reinforces the idea that it is related to a change in the viewing angle of the satellite.

There are two key characteristics that are more apparent in the SES 1 data. The first is the ringing in the polarization fractions of  $S_1$  and  $S_2$ . The second is how in the December data the values for polarization fractions of  $S_1$  and  $S_2$  showed many small features despite the fluxes indicating a

rather smooth distribution. These characteristics suggest that there is information about the structure and movement of the satellite that cannot be seen by just looking at the fluxes in different filters, but is revealed by the Stokes parameters.

### 3.2.3 Polarimetry of DirecTV 8

The polarimetric data results for DirecTV 8 are shown in Figure 3.9. The rows of the figure show data taken in October, December, and May. It is again important to note how the signature changes throughout the year. Originally in October, there is a broad peak with two very small, but symmetric side peaks. In the subsequent nights, the height of the major peak diminishes which then makes additional features more prominent. Thus, in the May data which is shown in Figure 3.9(g), the two minor peaks are now shoulders on the side of the major peak. The high side peak in Figure 3.9(d) is a result of a more direct reflection of light off of a piece of the satellite. However, it is still unclear exactly what type of satellite component would create this feature.

The trends for the  $S_1$  and  $S_2$  polarization fractions are similar to the other satellites. Like all the other satellites, the slope of the  $S_2$  polarization fraction is negative in the May data which continues to support the idea that this is caused by the viewing angle of the satellite. The most notable feature of the plots for the polarization fraction is the ringing that occurs each night. For most of the night the ringing is rather small in amplitude. However, located at  $\pm 30^\circ$  phase angle in Figure 3.9(b), there is a large spike in the polarization fraction. These spikes also correspond to the location of the side peaks that are seen in Figure 3.9(a). This means that whatever the light is reflecting off of at that point, it is polarizing the light much more than the main satellite structure. The ringing in the polarization fraction also shows the same trend as seen for SES 1 where it begins in the same direction for  $S_1$  and  $S_2$  and then goes in the opposite direction in the second half of the night.

The trends for the position angle and eccentricity shown in Figures 3.9(c), 3.9(f), and 3.9(i) also are similar to those for the other satellites. However, there are many small variations in the

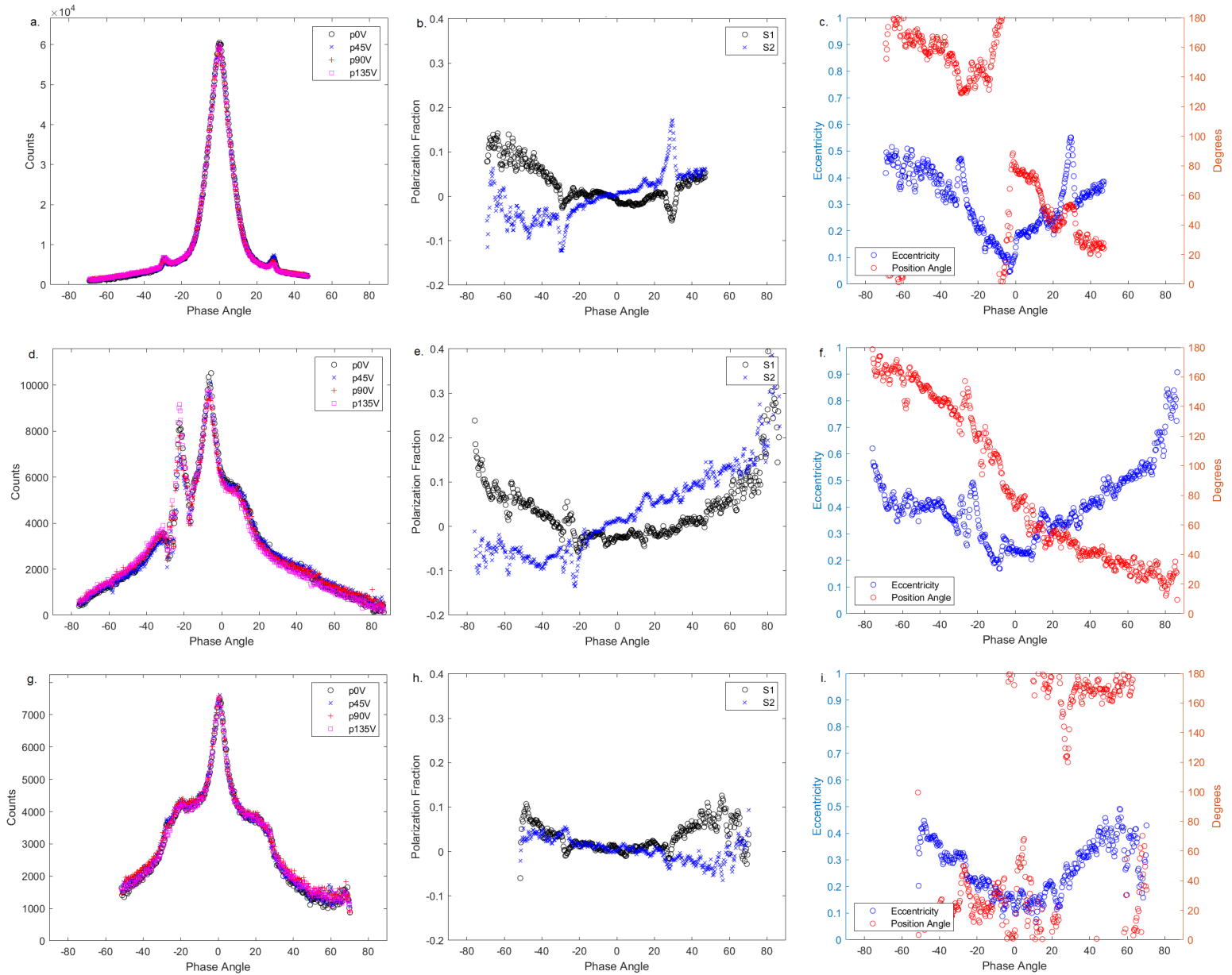


**Figure 3.9** Polarimetric data for DirecTV 8. Each plot shows values plotted against the phase angle. Plots (a)-(c) are for data taken in October, (d)-(f) are for December, and (g)-(i) are for May. Plots (a),(d),and (g) show the flux in each of the four polarized filters; (b),(e), and (h) are the calculated Stokes parameters  $S_1$  and  $S_2$ ; and (c),(f), and (i) show the position angle as well as eccentricity. It is important to note how the light coming off the side peaks in Plot (a) is much more polarized as seen by the spikes in polarization fractions and eccentricity in Plots (b) and (c).

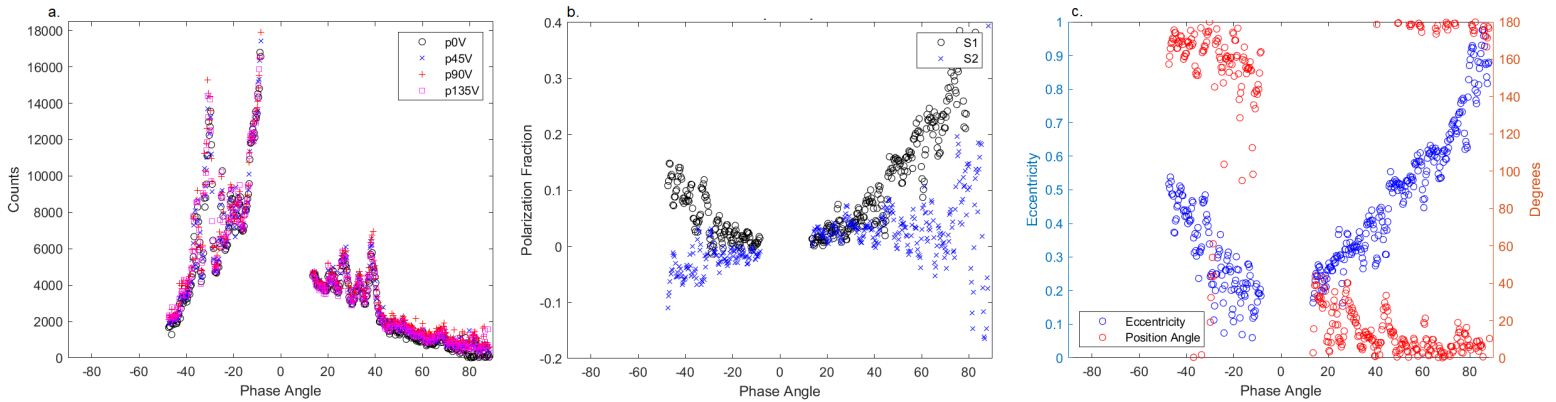


**Figure 3.10** Polarimetry results for DirecTV 4. The flux,  $S_1$  and  $S_2$  polarization fractions, eccentricity, and position angle are plotted against phase angle. Plot (a) shows a complex signature with many peaks of various intensities. This then creates a similarly complex signature for the polarization fractions seen in Plot (b). Despite these complexities, the eccentricity and position angle variation shown in Plot (c) is much smoother.

eccentricity as a result of the ringing in the polarization fractions. As might be expected, there are also two spikes in the eccentricity shown in Figure 3.9(c) which correspond to the peaks in Figures 3.9(a) and 3.9(b). This is another sign that the light at those points of the night was polarized to a greater degree. The position angle in each night varies from about  $160^\circ$  to  $20^\circ$  with varying degrees of smoothness. The same flip in the position angle trend is seen in Figure 3.9(i) that has been seen for the other satellites.

### 3.2.4 Polarimetry of DirecTV 4

Perhaps the most interesting signature comes from DirecTV 4. This satellite was only observed in September. For the other satellites, their September signature was quite smooth and showed very few features. DirecTV 4 does not follow this trend. Beginning with Figure 3.10(a), numerous narrow peaks in flux occur throughout the night. The primary peak occurs near  $-10^\circ$  phase angle and at least five other minor peaks appear at various phase angles. Given, the complexity of this signature, it is much more difficult to understand what about the structure of the satellite is creating

all these spikes in the flux as light is reflected off it.

Figure 3.10(b) showing the polarization fraction for the Stokes parameters is just as complex as the flux plot. The  $S_1$  polarization fraction does vary in a parabolic fashion. It begins at a fraction of 0.17, drops to near 0, and then increases up towards 0.4 by the end of the night. The trend for  $S_1$  is less clear, but still appears to be linear with a positive slope. The most noticeable characteristic of this plot is the large amounts of higher frequency ringing. Since the oscillations are happening so quickly, it is difficult to say for certain if the oscillations between  $S_1$  and  $S_2$  are in or out of phase with each other. Both parameters converge close to 0 at  $-10^\circ$  phase angle which does coincide with where the main peak in the flux data occurs.

Despite some of the chaotic nature of the first two plots, the eccentricity seems to vary more smoothly. The variation is roughly parabolic and ranges from 0.2 up to between 0.9 and 1 at the end of the night. This means that at the end of the night the light was almost completely linearly polarized. The position angle does vary less smoothly, but the overall trend is that it decreases from  $170^\circ$  to very near  $0^\circ$  by the end of the night.

Overall, all the satellites showed unique characteristics in their fluxes, Stokes parameters, and eccentricity and phase angle. Variations throughout the year are largely a result of the changing satellite viewing angle. It is still unclear what causes the ringing so prevalent throughout some of the nights and especially for DirecTV 4. In order to understand how the satellite structure and movement is reflected in the polarized data, additional nights of observation are needed as well as additional analysis.

### 3.3 Conclusion

One of the first conclusions of this research is that standard astronomical techniques can be used to create signatures for GEO satellites. As shown these signatures are unique to the satellite and can

be used to identify and monitor the satellite. Since the signature does depend on the viewing angle of the satellite, multiple nights of observation are needed in order to fully characterize the signature of a particular satellite.

While looking at evidence for space aging, it was found that satellites exhibited both reddening and dimming. However, different satellites did not exhibit these signs in the same way. What was found was that some satellites showed signs of reddening while others showed dimming. There was also a case where neither reddening nor dimming was seen. When seen, the dimming was equal to approximately 0.1 magnitudes, and the reddening was equal to a shift in color index by about 0.1. The differences in aging are most likely a result of the different materials used to construct the satellites.

Finally, polarimetric data for four satellites was shown and characterized. It is clear that the polarimetric data contains additional information that is not present in the photometric data alone. For example, in Figure 3.8, the plots of the fluxes showed very few features, while the plots for the polarization fractions showed ringing in the fractions occurring throughout the night. Given this result, it is clear that by studying the satellites using polarimetry, we will be able to identify aspects about the satellites movements and structure that otherwise could not be found by photometry alone.

One major feature seen is a flip in the flux ordering throughout the night. This flip occurs such that the slope of the  $S_2$  polarization fraction is positive from September to March. Then when data was taken in May the trend for  $S_2$  changes so that throughout the night it had a negative slope. The exact reason for this change is currently unclear. However, we believe that it is caused by the change in the viewing angle of the satellite. Since the viewing angle changes from positive to negative at the spring equinox it is possible that it could create this flip.

Another main feature that was seen in some of the satellites was ringing in the polarization fractions. It is still unclear what causes this ringing. However, given its oscillatory nature, it is unlikely that it is a result of the materials. More likely, it is caused by movements or flexing done by

the satellite that occur throughout the night which change how much the light is being polarized. It is also puzzling how the oscillations for  $S_1$  and  $S_2$  are in phase for half the night and out of phase for the other half. This feature clearly needs more data and analysis in order to understand what is causing it.

There is obviously a wealth of information contained within the polarization data for these satellites. However, we are still in the early phases of understanding what is causing the features that are observed in the polarization plots. The first two features that we hope to be able to understand are the ringing and the flip in  $S_2$  that is seen in every satellite. As we perform some simple experiments, we are hopeful that we will be able to understand these features and then move on to other characteristics of the satellites. Eventually, as we continue this work we should be able to characterize the satellite, understand their structures, and be able to identify any maneuvers they make.

### 3.4 Further Work Needed

There are still several areas where work needs to be continued. First, as mentioned the signatures change throughout the year. For many of the satellites, observations have only been taken during one summer. In order for this work to be truly useful in identifying and monitoring satellites, additional observations need to be taken in order to have a complete year of data for each satellite. Likewise, data were only collected for a handful of satellites with fewer being observed using polarized filters. An important next step will be to observe a wider range of GEO satellites using both photometry and polarimetry.

When looking at the signs of space aging, it will also be necessary to monitor the satellites over an even longer time frame. This will help us gain an understanding about when certain signs of aging appear and to what degree they are manifested. In addition to this, the primary materials that

make up the satellites need to be studied. This will allow us to understand what type of aging should be expected by different satellites based on their composition.

With all the signatures and calculated quantities like the Stokes parameters, multiple effects are being seen at once. In a single night, materials, movement, and phase angle help create the results seen. Then throughout the year, the changes in satellite viewing angle also changes the results obtained. In order to be able to identify and characterize satellites and their movements based on their photometric signatures and polarimetric parameters, additional observations and experiments are needed. These will help us understand which variations are the result of the multiple factors like phase angle, material, and viewing angle.

One such experiment that could be performed would be to test how the trend for the  $S_2$  polarization fractions change with different viewing angles. For this experiment, a tilted solar panel could be illuminated and rotated through different angles to simulate the changing phase angle. The reflected light could then be passed through a linearly polarized filter and recorded by a photodiode. The filter would then be rotated so the flux at  $0^\circ$ ,  $45^\circ$ ,  $90^\circ$ , and  $135^\circ$  could be found which would allow the Stokes parameters to be calculated. If the change in the slope of the  $S_2$  trend is caused by the viewing angle, then this experiment should be able to replicate the result.

# Appendix A

## Additional Satellite Plots

### A.1 DirecTV 9S Plots

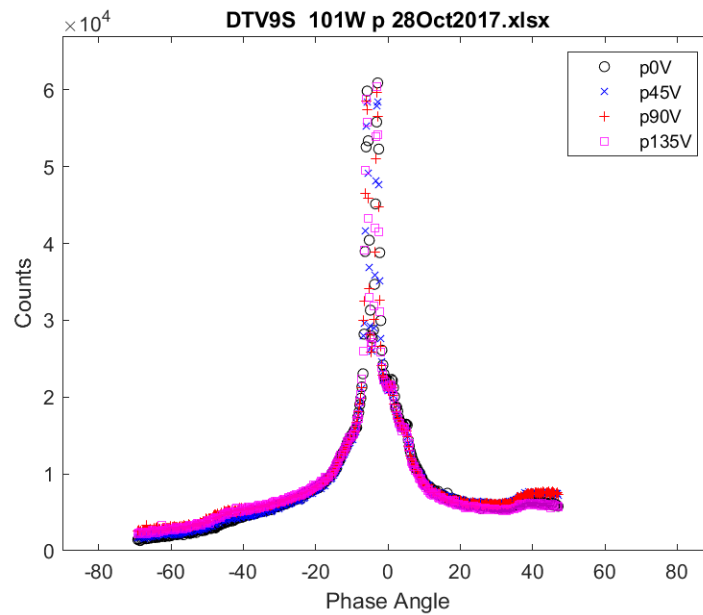


**Figure A.1** DirecTV 9S counts for 28 October 2017

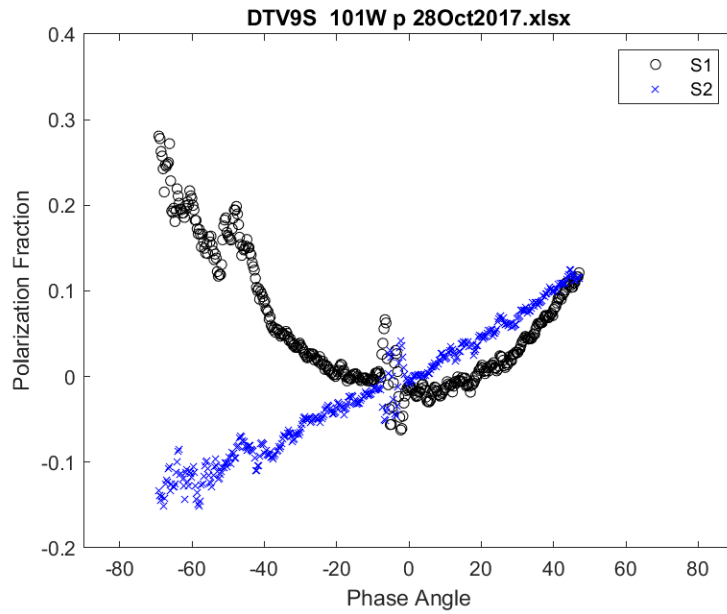


Figure A.2 DirecTV 9S  $S_1$  and  $S_2$  polarization fractions for 28 October 2017

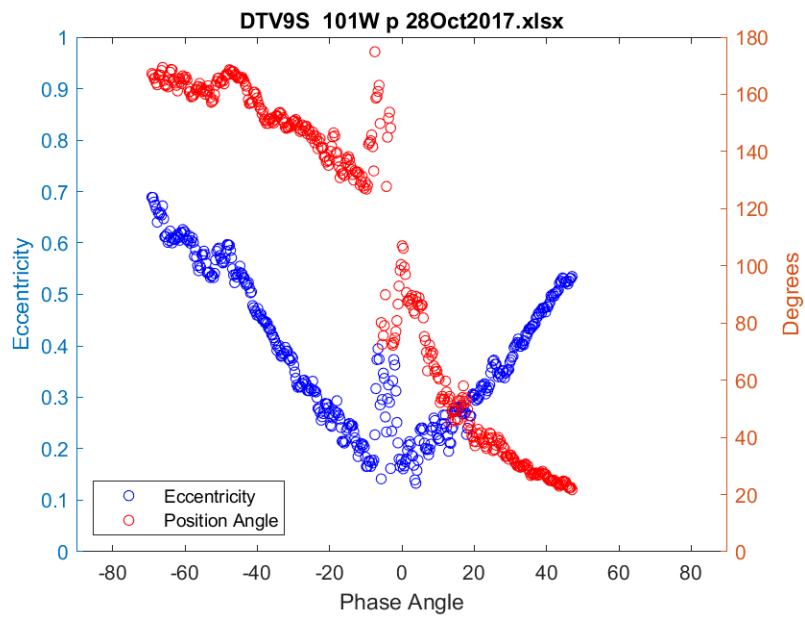
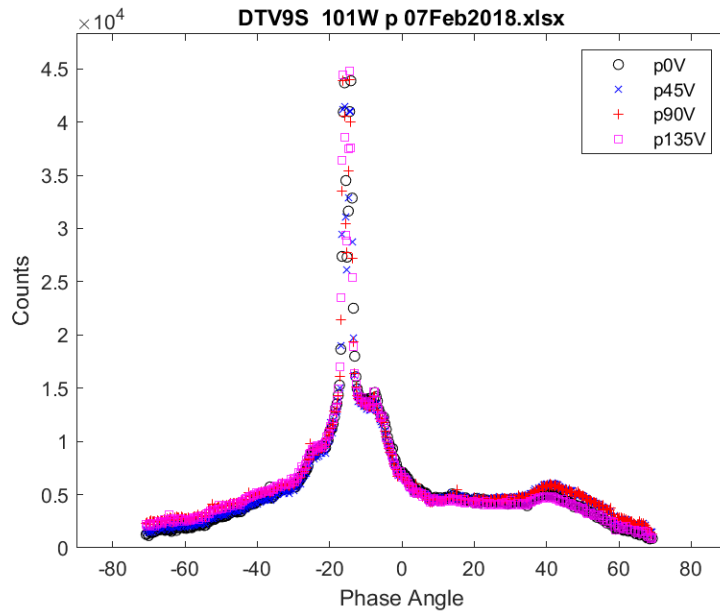
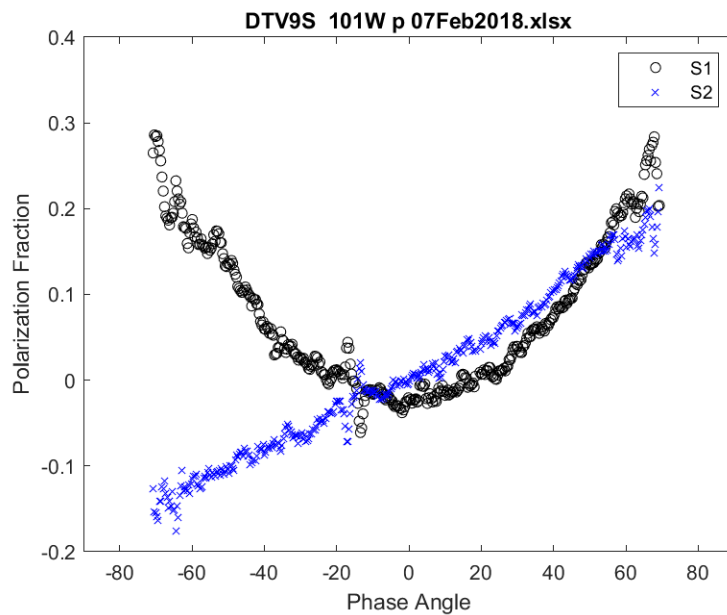


Figure A.3 DirecTV 9S eccentricity and position angle for 28 October 2017



**Figure A.4** DirecTV 9S counts for 7 February 2018



**Figure A.5** DirecTV 9S  $S_1$  and  $S_2$  polarization fractions for 7 February 2018

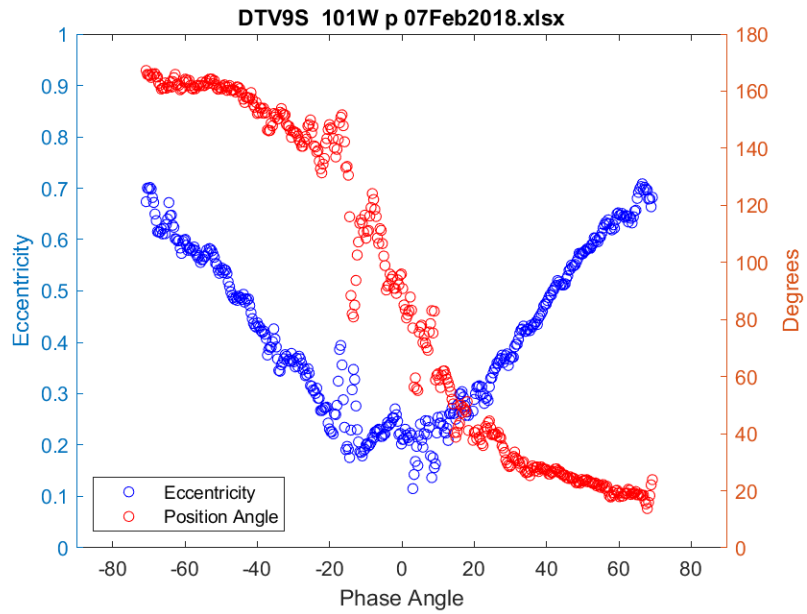


Figure A.6 DirecTV 9S eccentricity and position angle for 7 February 2018

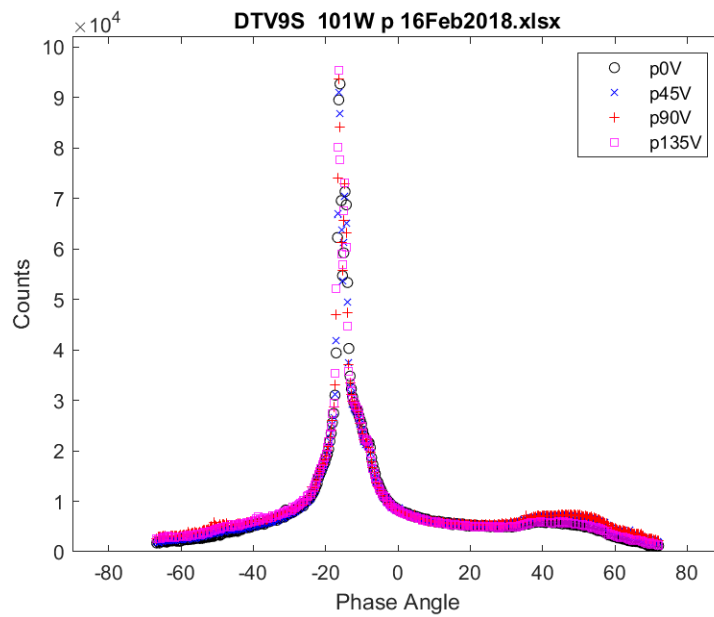
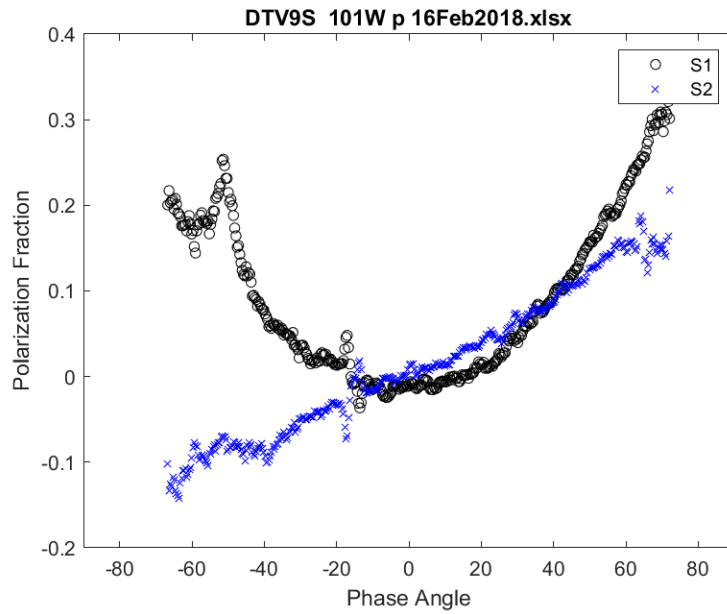
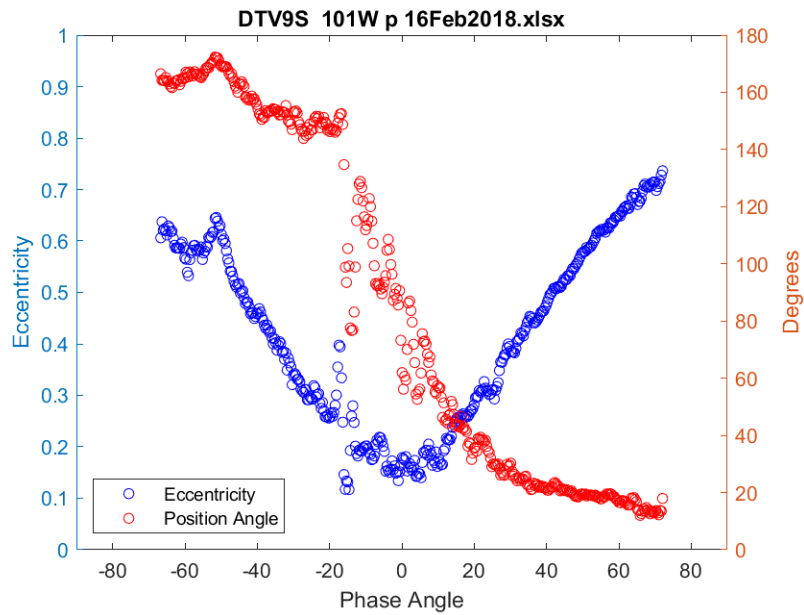


Figure A.7 DirecTV 9S counts for 16 February 2018



**Figure A.8** DirecTV 9S  $S_1$  and  $S_2$  polarization fractions for 16 February 2018



**Figure A.9** DirecTV 9S eccentricity and position angle for 16 February 2018

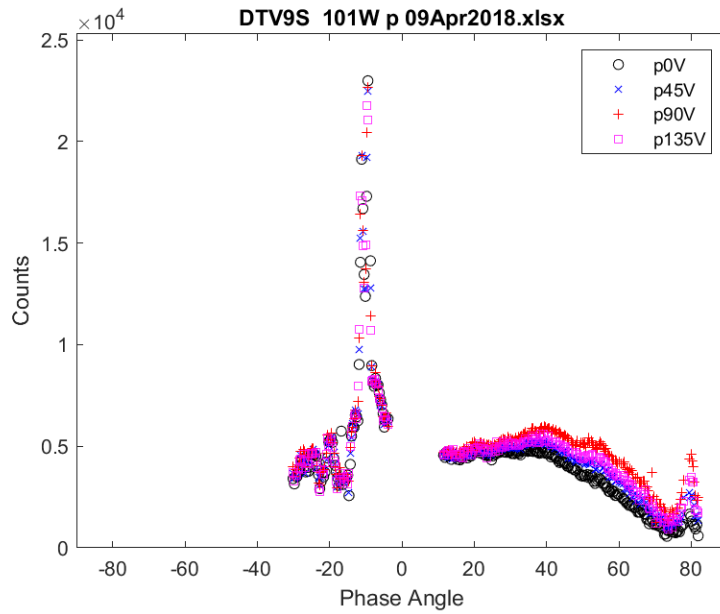


**Figure A.10** DirecTV 9S counts for 9 April 2018

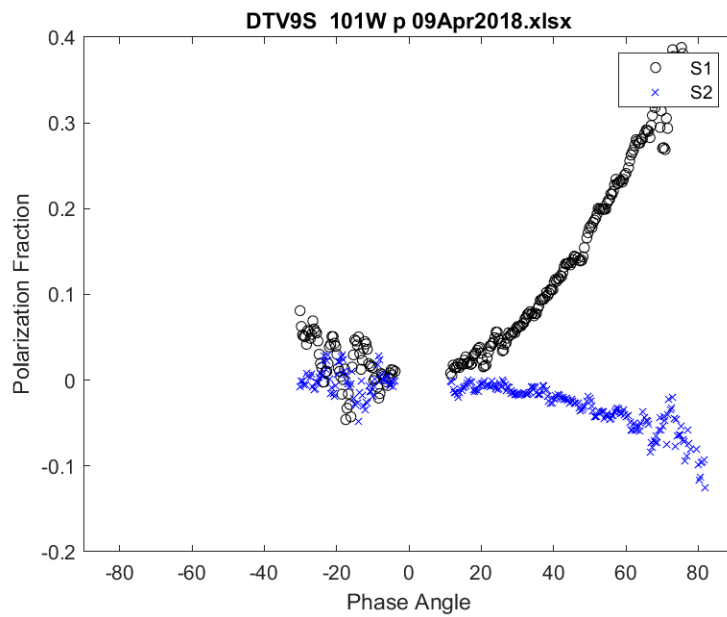


**Figure A.11** DirecTV 9S  $S_1$  and  $S_2$  polarization fractions for 9 April 2018

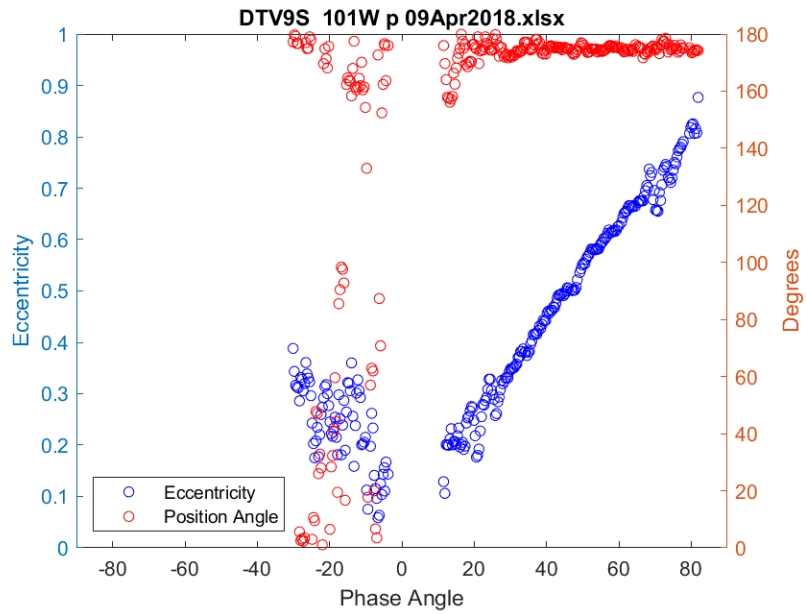


**Figure A.12** DirecTV 9S eccentricity and position angle for 9 April 2018

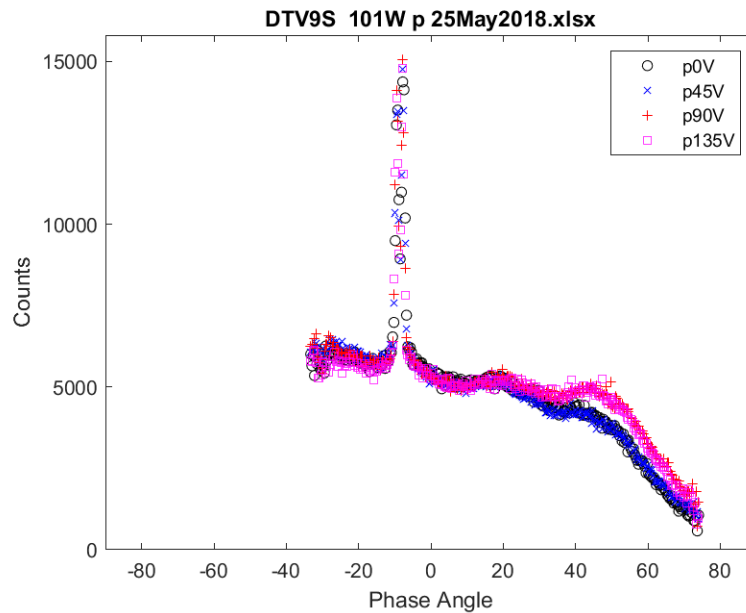


**Figure A.13** DirecTV 9S counts for 25 May 2018

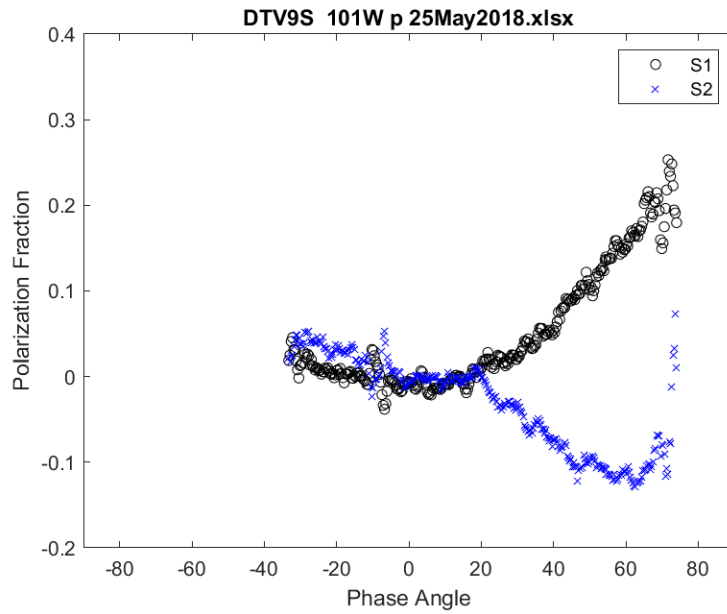


**Figure A.14** DirecTV 9S  $S_1$  and  $S_2$  polarization fractions for 25 May 2018

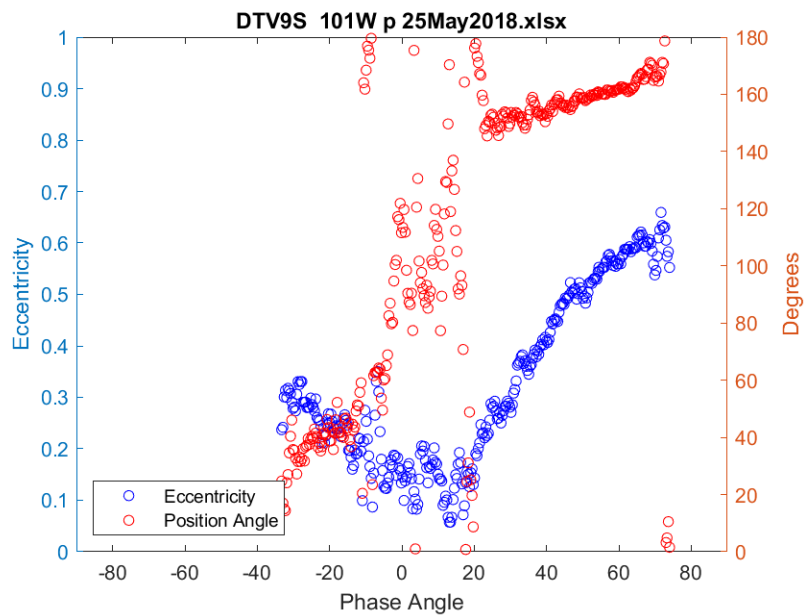


**Figure A.15** DirecTV 9S eccentricity and position angle for 25 May 2018

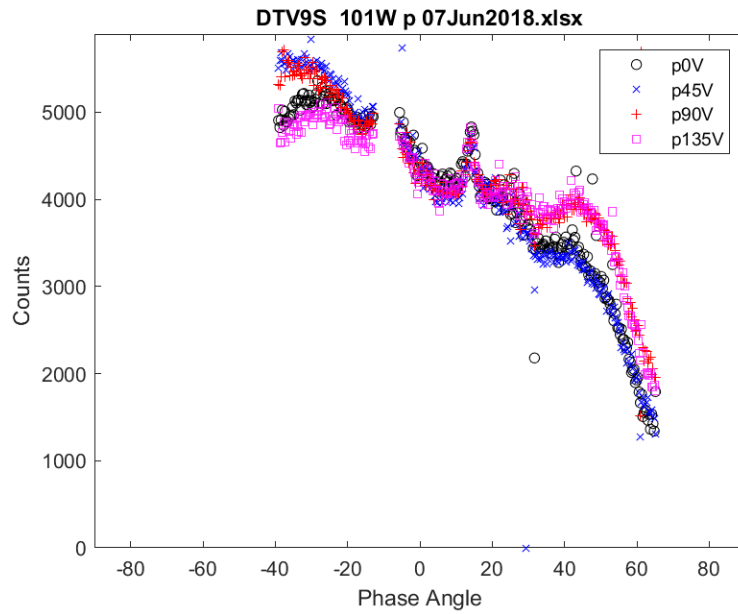


**Figure A.16** DirecTV 9S counts for 7 June 2018

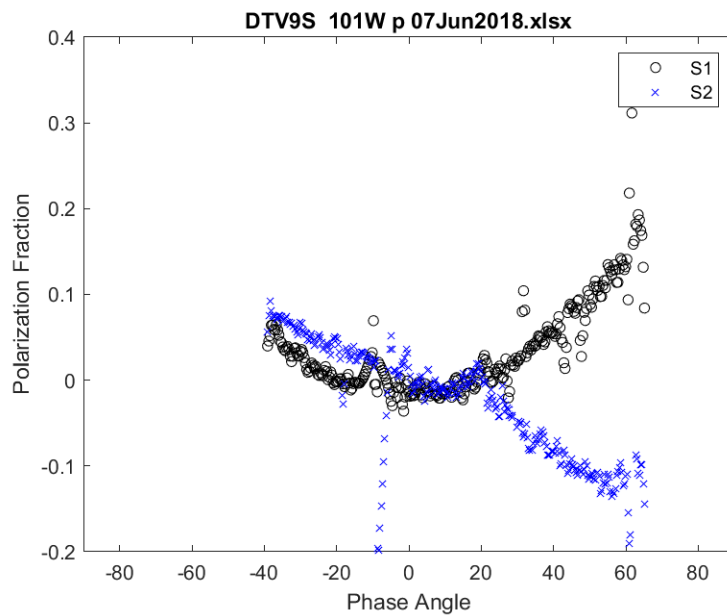


**Figure A.17** DirecTV 9S  $S_1$  and  $S_2$  polarization fractions for 7 June 2018

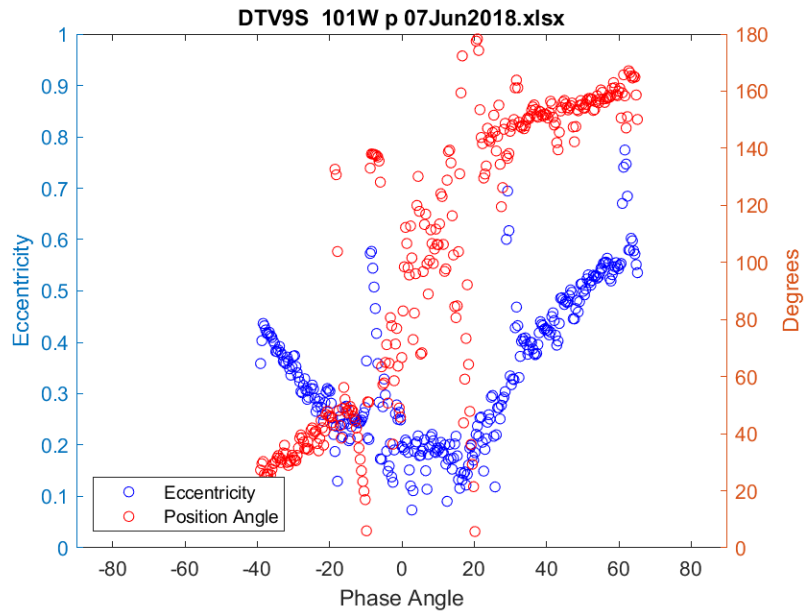


Figure A.18 DirecTV 9S eccentricity and position angle for 7 June 2018

## A.2 SES 1 Plots

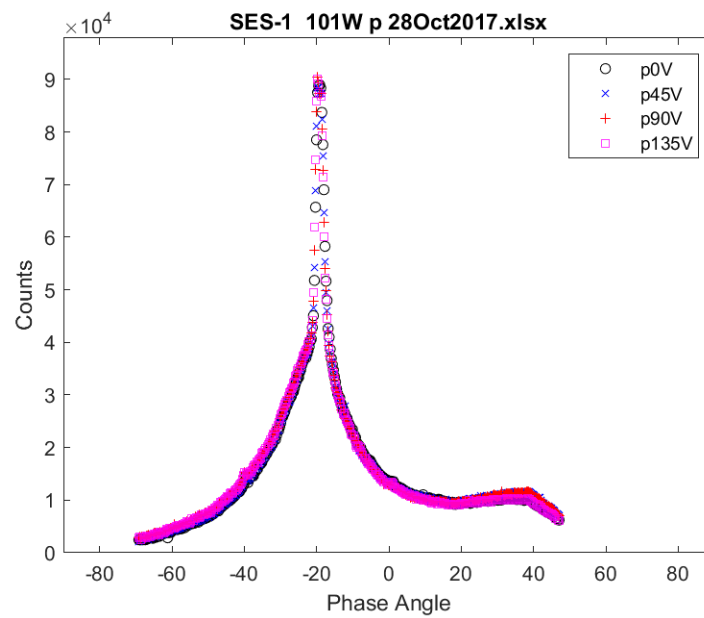
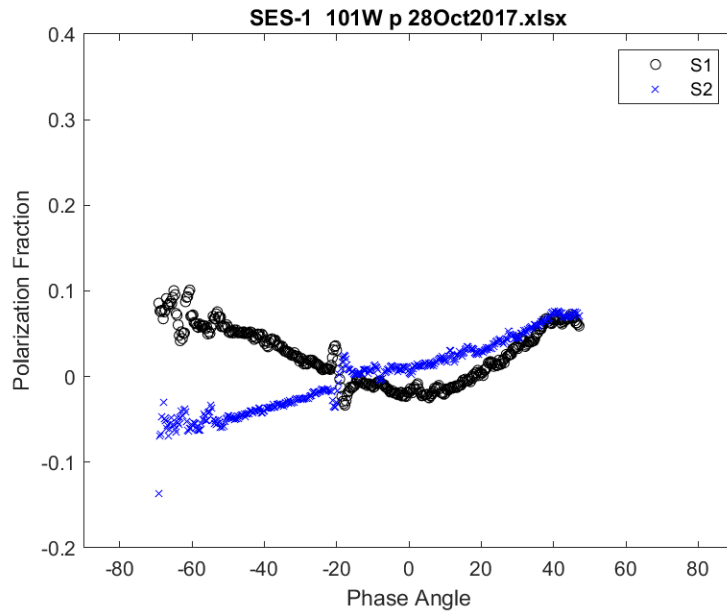
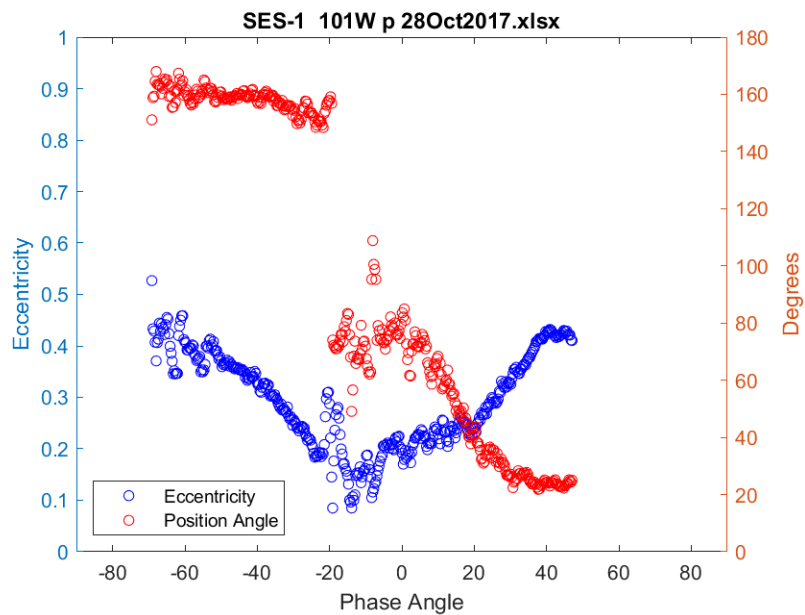


Figure A.19 SES 1 counts for 28 October 2017



**Figure A.20** SES 1  $S_1$  and  $S_2$  polarization fractions for 28 October 2017



**Figure A.21** SES 1 eccentricity and position angle for 28 October 2017

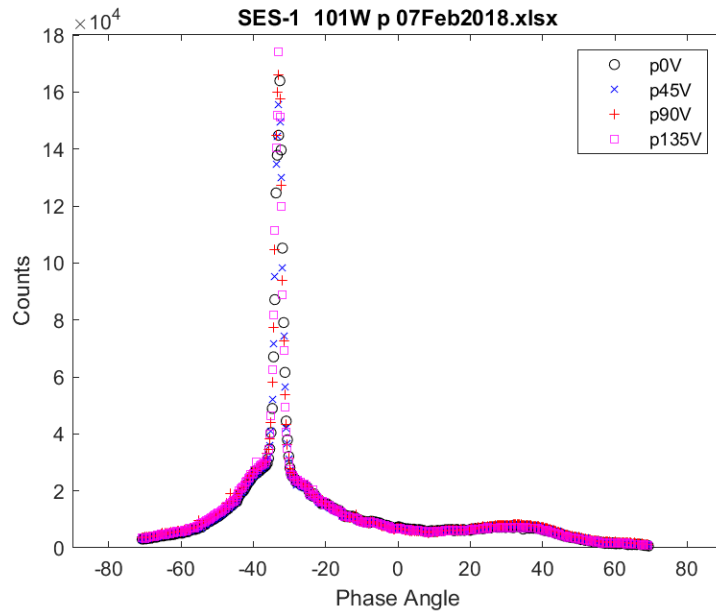


**Figure A.22** SES 1 counts for 7 February 2018

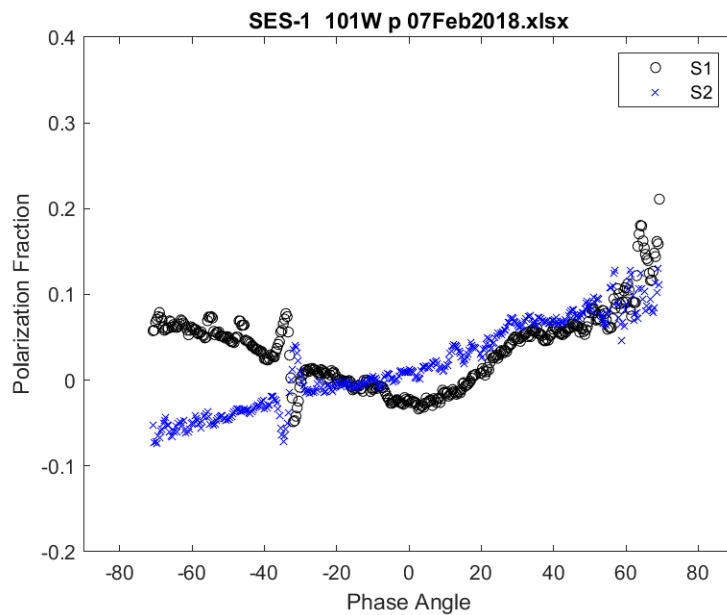


**Figure A.23** SES 1  $S_1$  and  $S_2$  polarization fractions for 7 February 2018

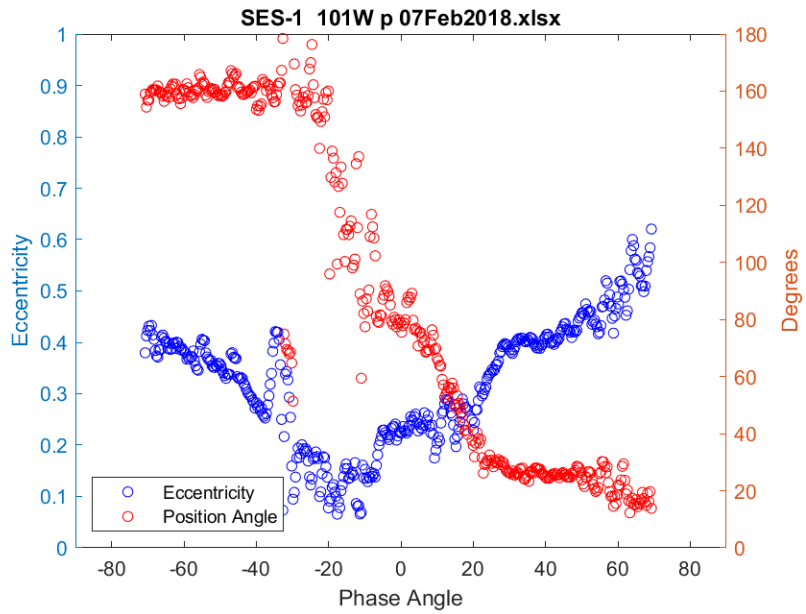


**Figure A.24** SES 1 eccentricity and position angle for 7 February 2018

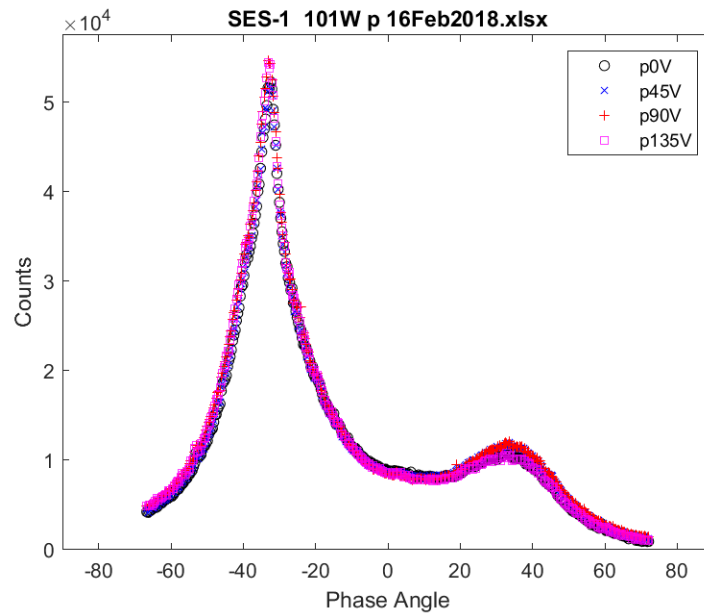


**Figure A.25** SES 1 counts for 16 February 2018

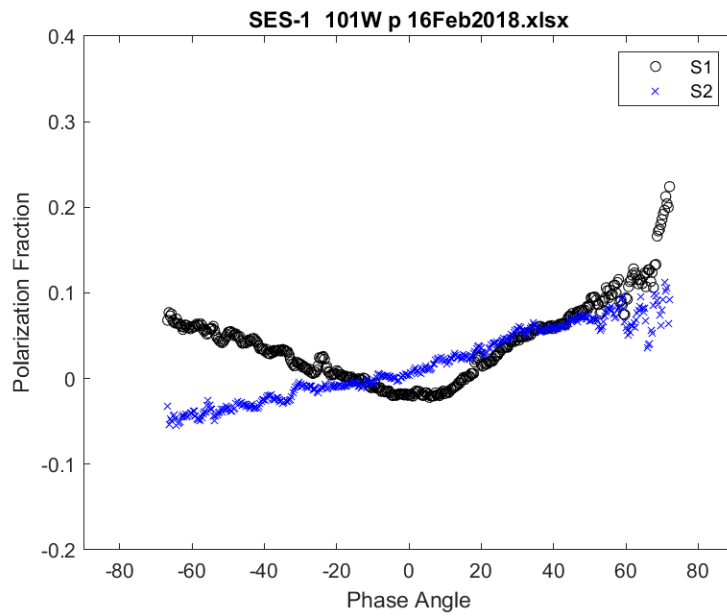


**Figure A.26** SES 1  $S_1$  and  $S_2$  polarization fractions for 16 February 2018

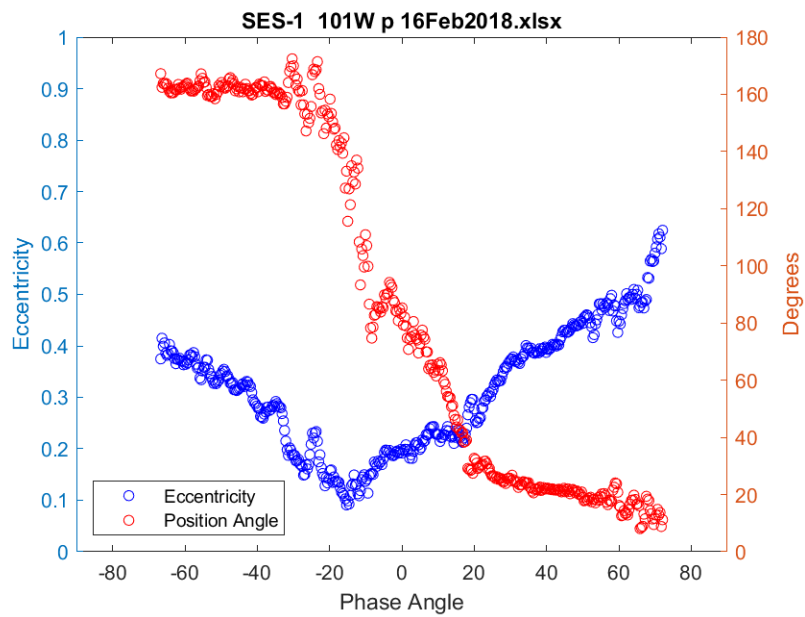


**Figure A.27** SES 1 eccentricity and position angle for 16 February 2018

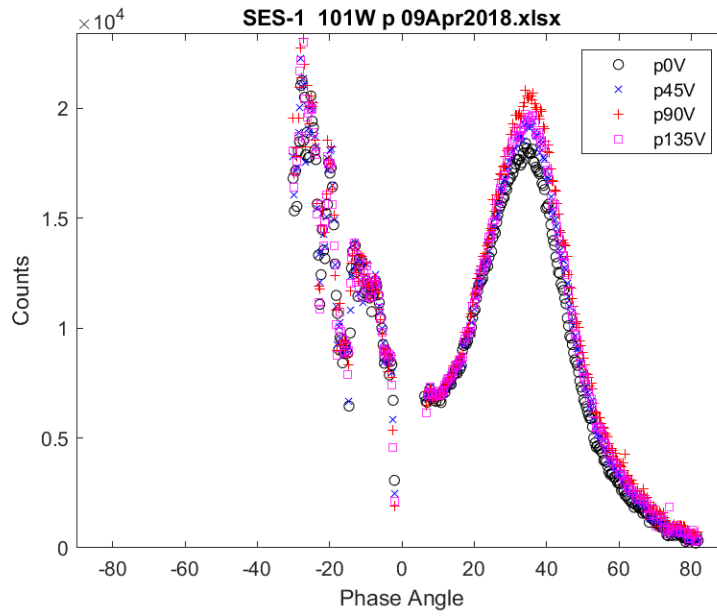


Figure A.28 SES 1 counts for 9 April 2018

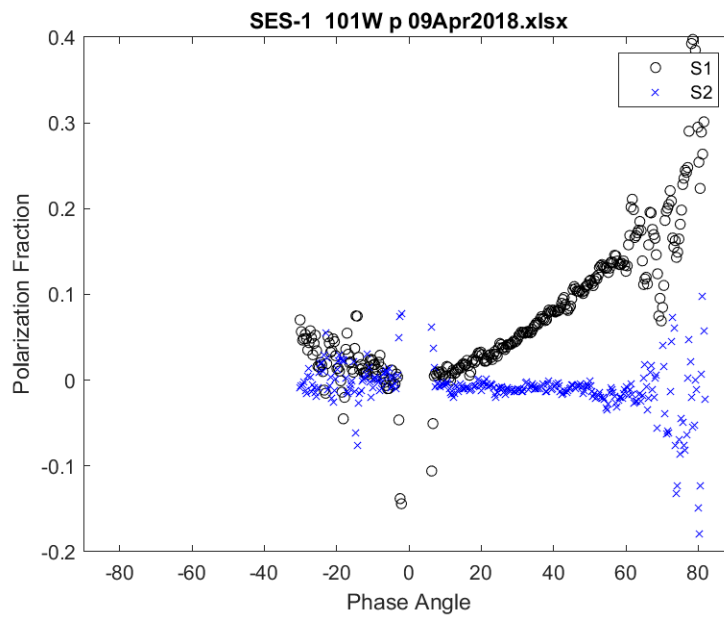
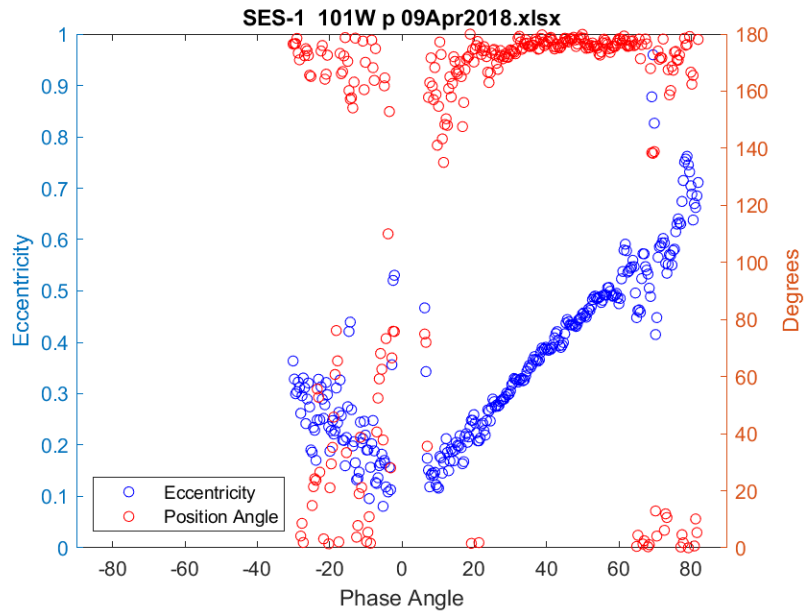
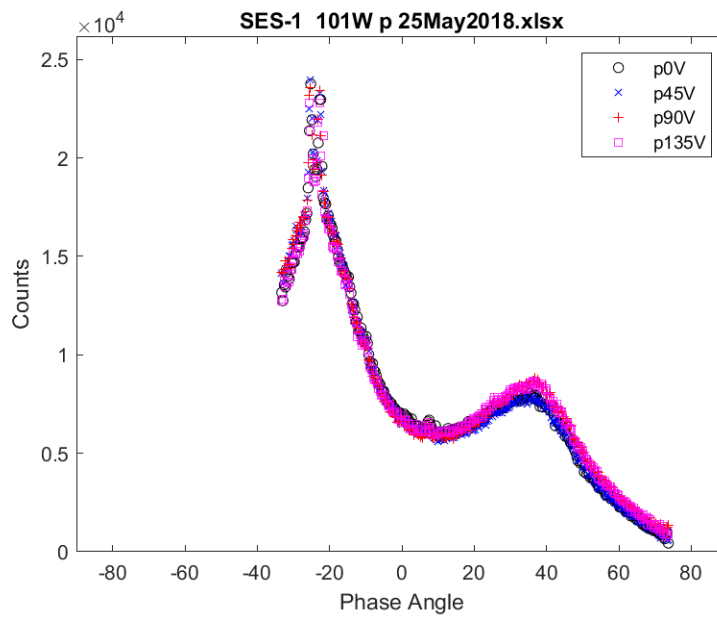


Figure A.29 SES 1  $S_1$  and  $S_2$  polarization fractions for 9 April 2018



**Figure A.30** SES 1 eccentricity and position angle for 9 April 2018



**Figure A.31** SES 1 counts for 25 May 2018

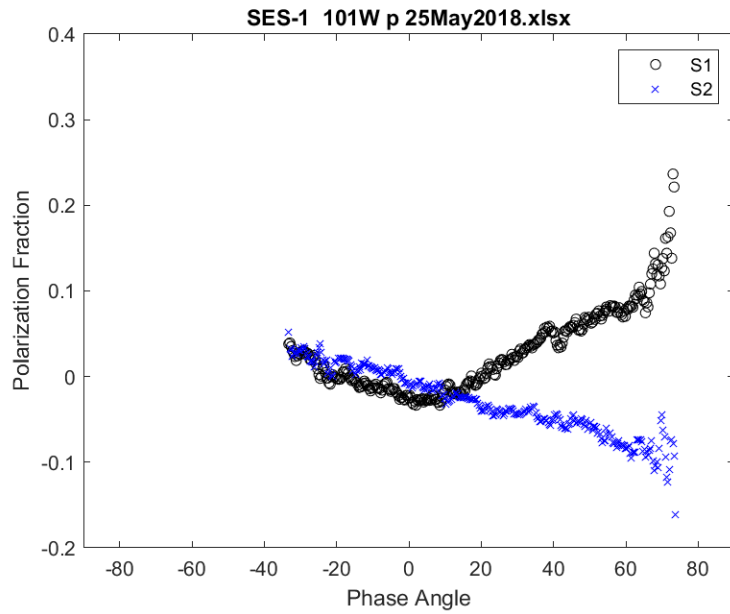


Figure A.32 SES 1  $S_1$  and  $S_2$  polarization fractions for 25 May 2018

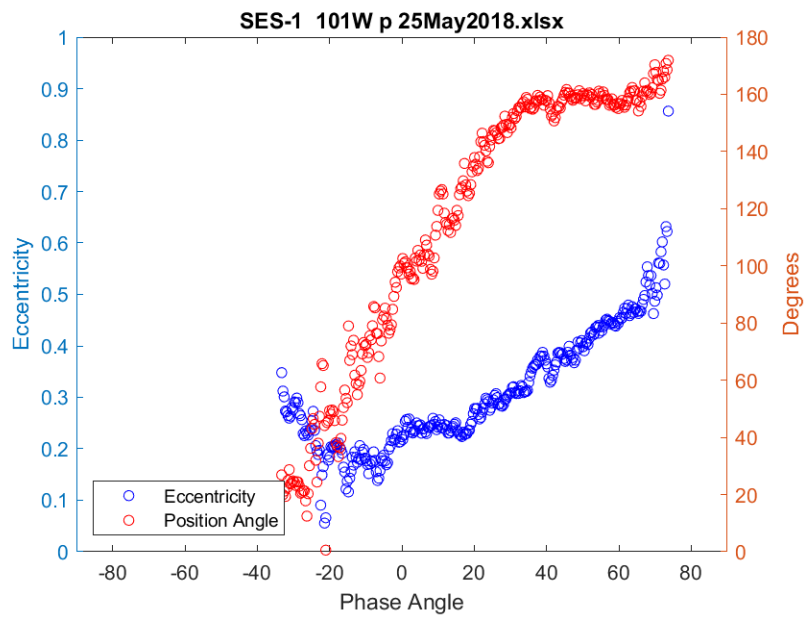


Figure A.33 SES 1 eccentricity and position angle for 25 May 2018

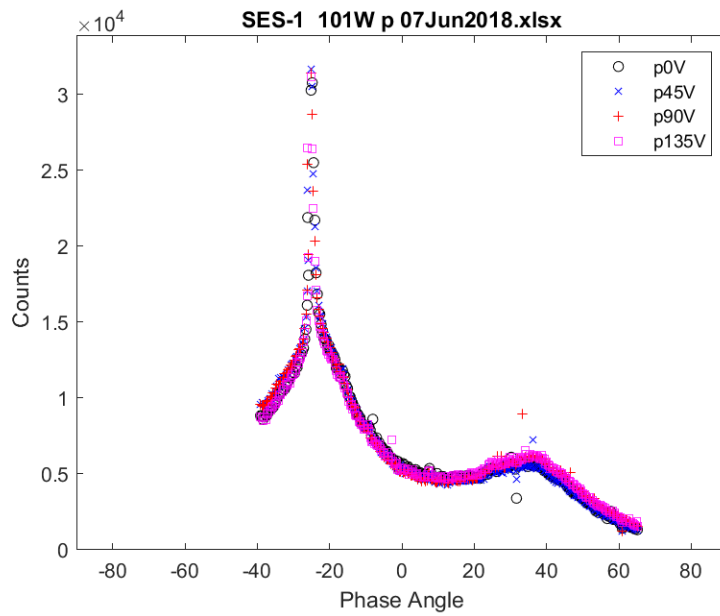


Figure A.34 SES 1 counts for 7 June 2018

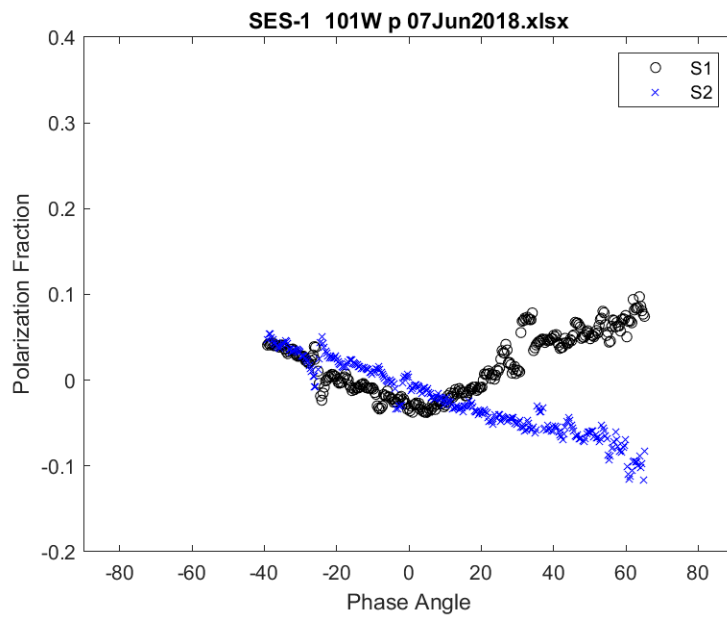


Figure A.35 SES 1  $S_1$  and  $S_2$  polarization fractions for 7 June 2018

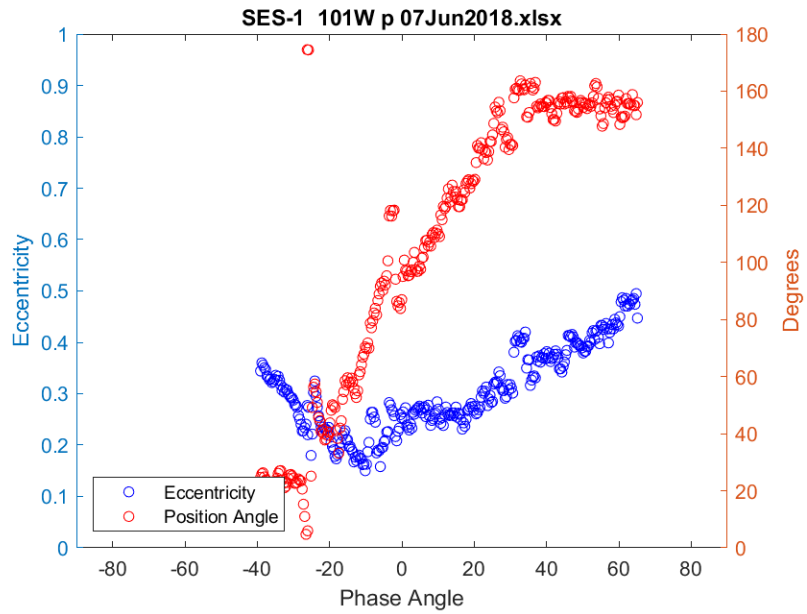


Figure A.36 SES 1 eccentricity and position angle for 7 June 2018

### A.3 DirecTV 8 Plots

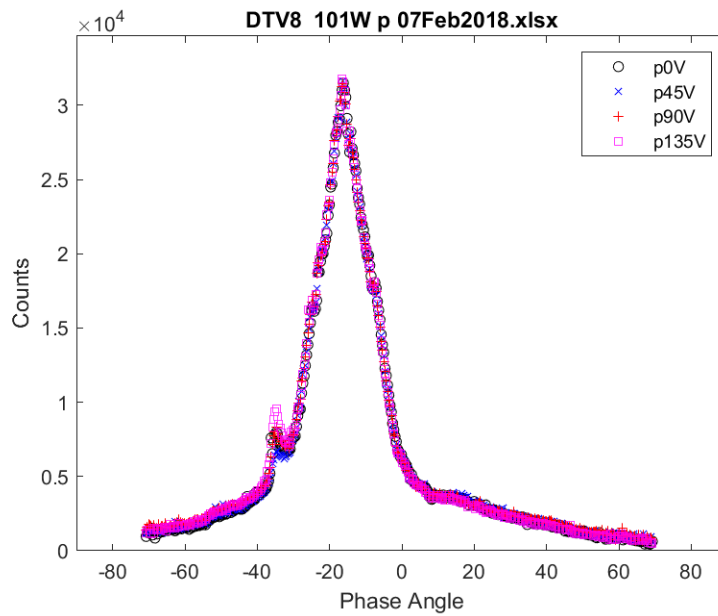


Figure A.37 DirecTV 8 counts for 7 February 2018

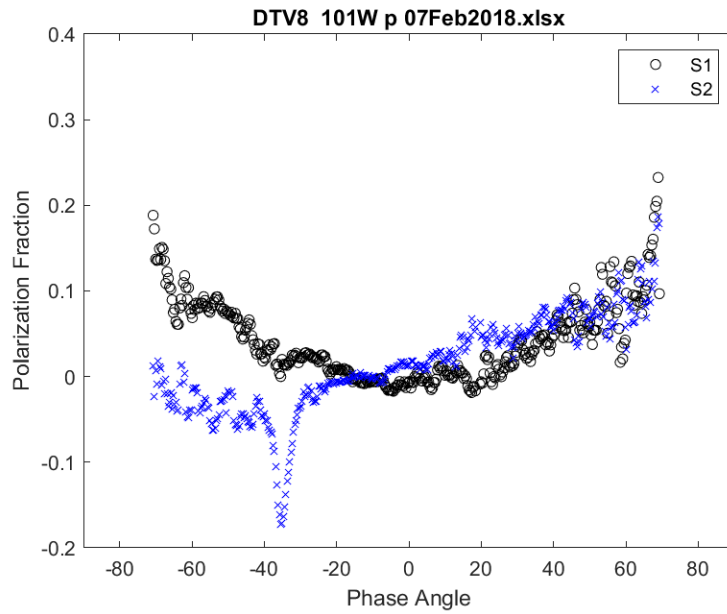


Figure A.38 DirecTV 8  $S_1$  and  $S_2$  polarization fractions for 7 February 2018

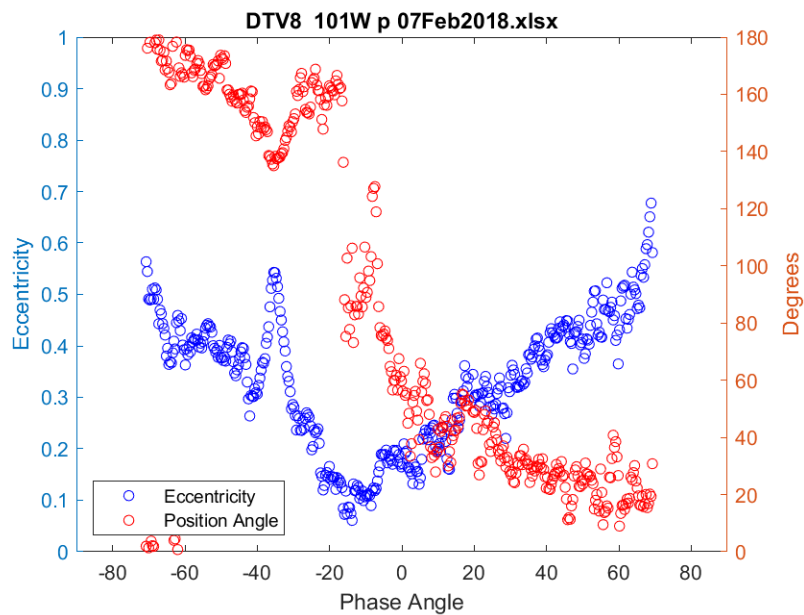
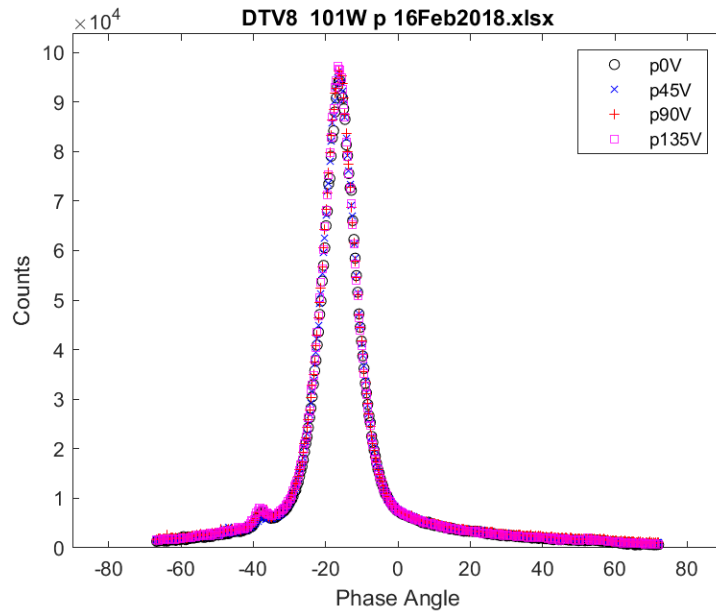
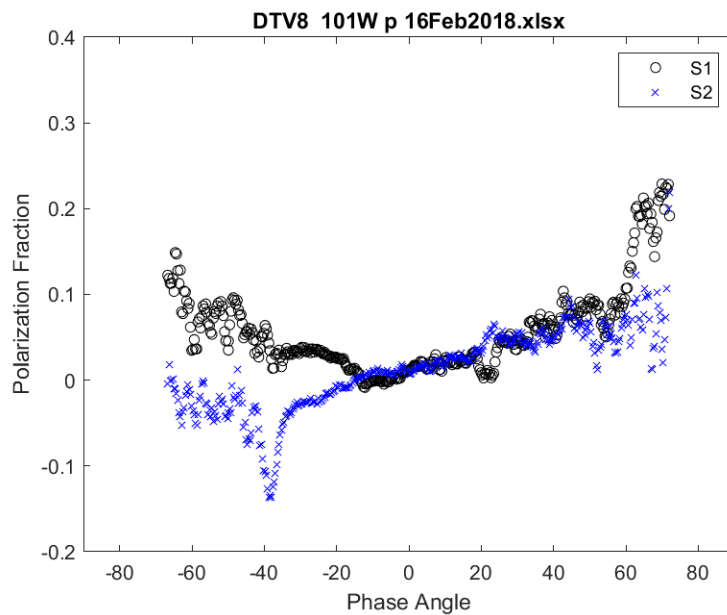


Figure A.39 DirecTV 8 eccentricity and position angle for 7 February 2018



**Figure A.40** DirecTV 8 counts for 16 February 2018



**Figure A.41** DirecTV 8  $S_1$  and  $S_2$  polarization fractions for 16 February 2018

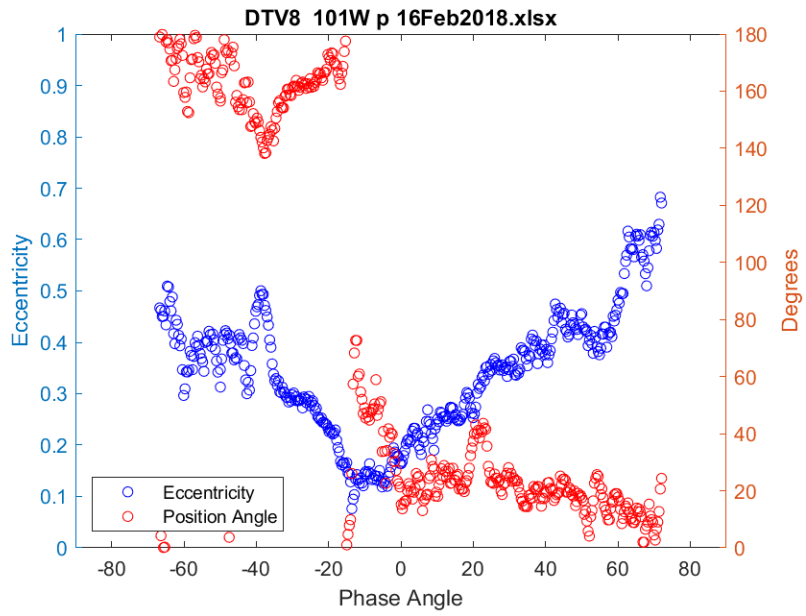


Figure A.42 DirecTV 8 eccentricity and position angle for 16 February 2018

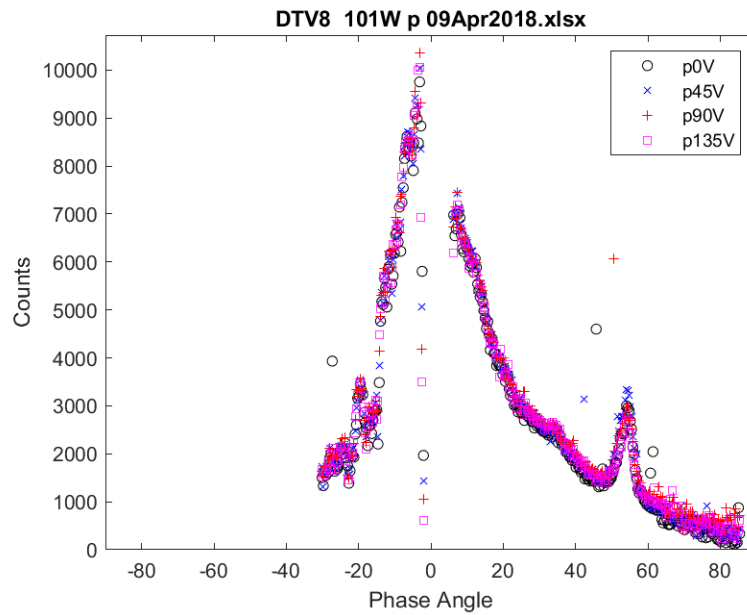
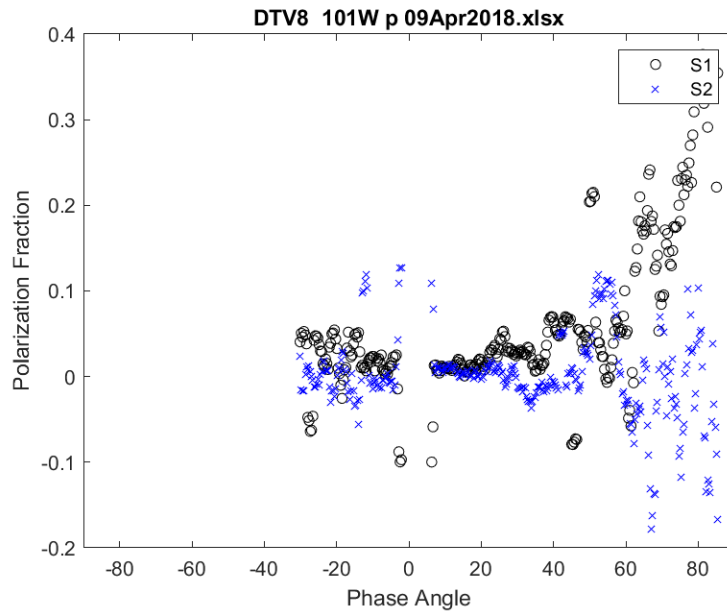
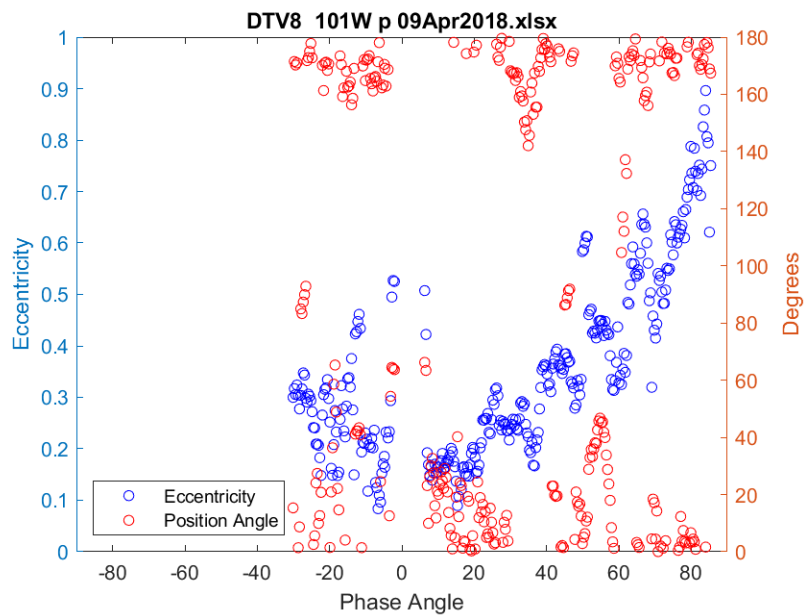


Figure A.43 DirecTV 8 counts for 9 April 2018



**Figure A.44** DirecTV 8  $S_1$  and  $S_2$  polarization fractions for 9 April 2018



**Figure A.45** DirecTV 8 eccentricity and position angle for 9 April 2018

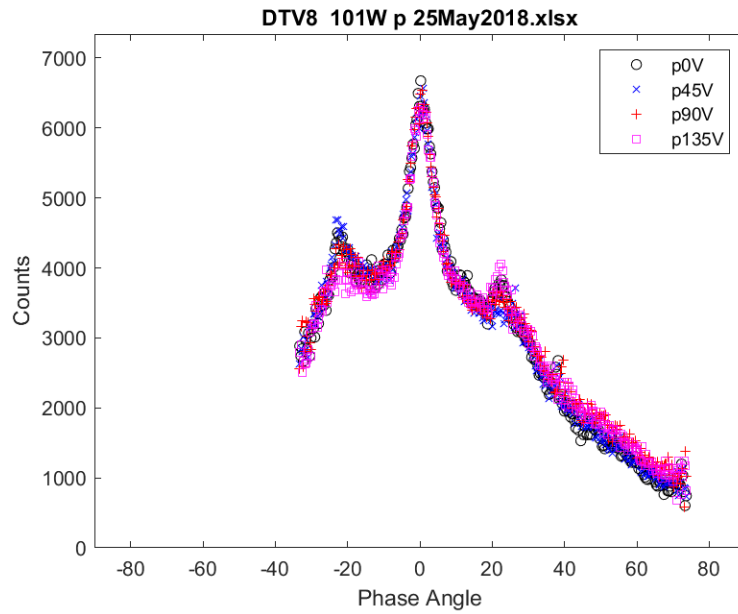


**Figure A.46** DirecTV 8 counts for 25 May 2018

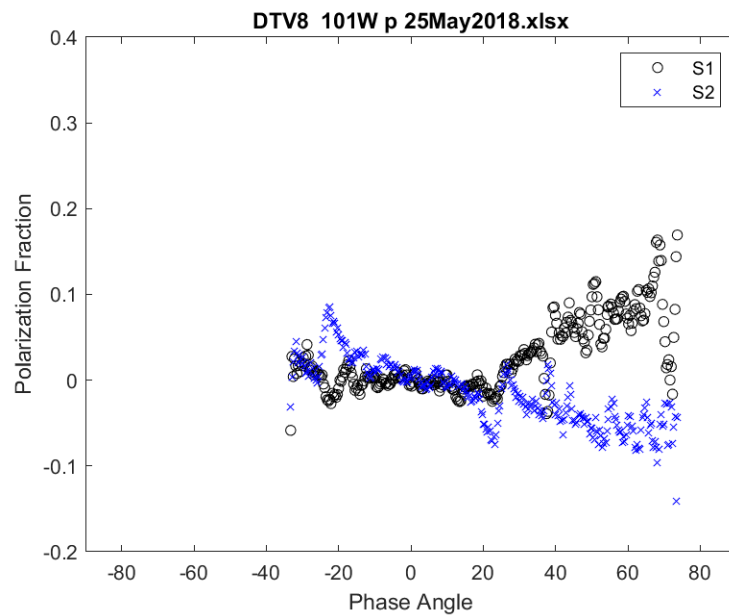


**Figure A.47** DirecTV 8  $S_1$  and  $S_2$  polarization fractions for 25 May 2018

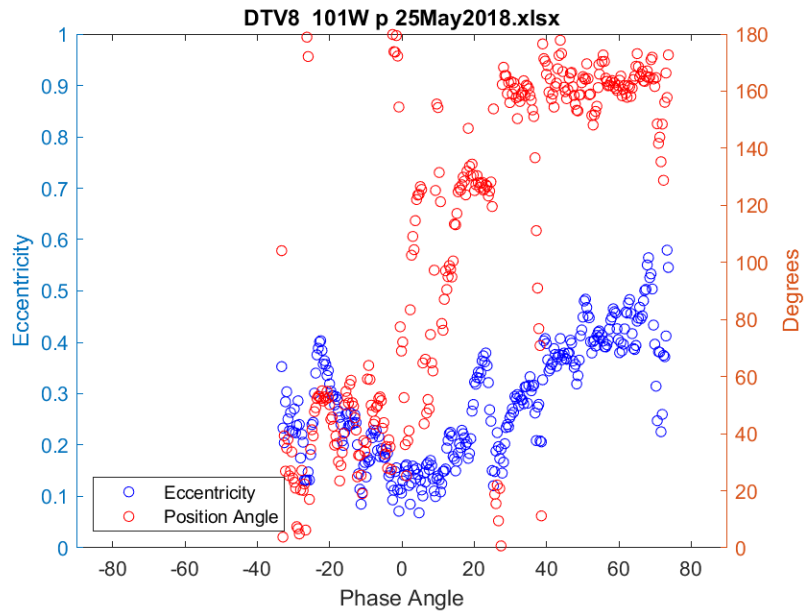


**Figure A.48** DirecTV 8 eccentricity and position angle for 25 May 2018

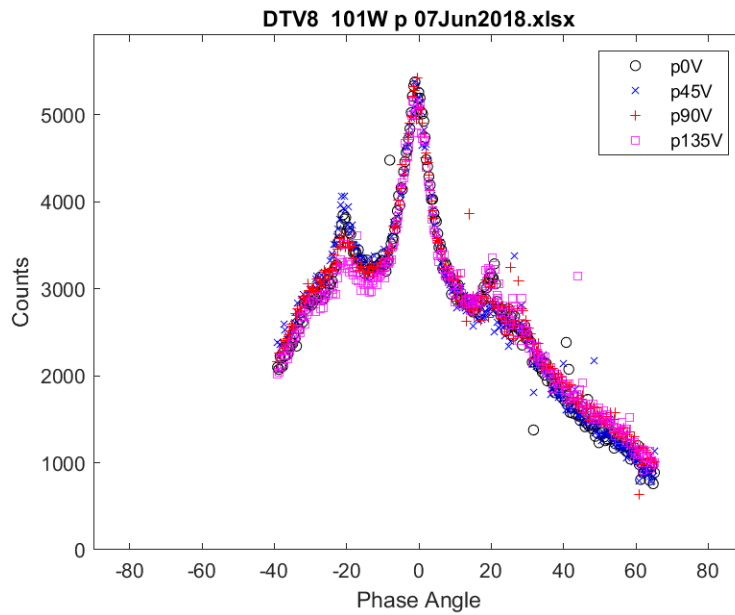


**Figure A.49** DirecTV 8 counts for 7 June 2018

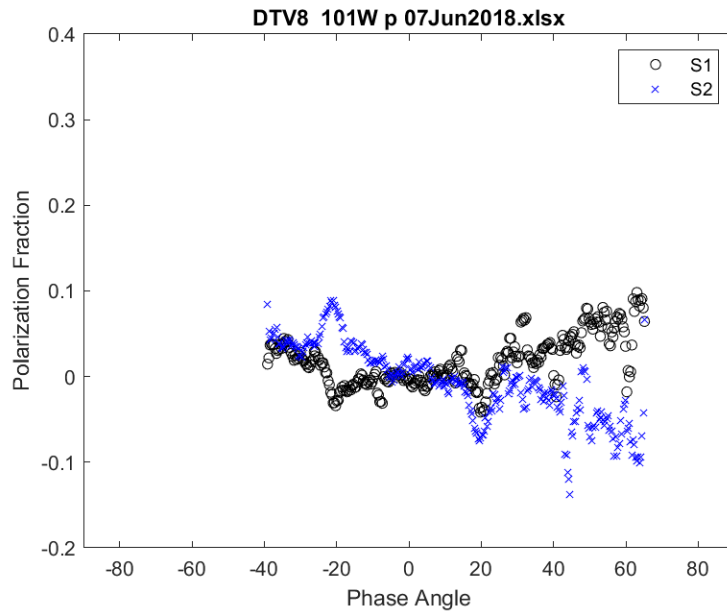


**Figure A.50** DirecTV 8  $S_1$  and  $S_2$  polarization fractions for 7 June 2018

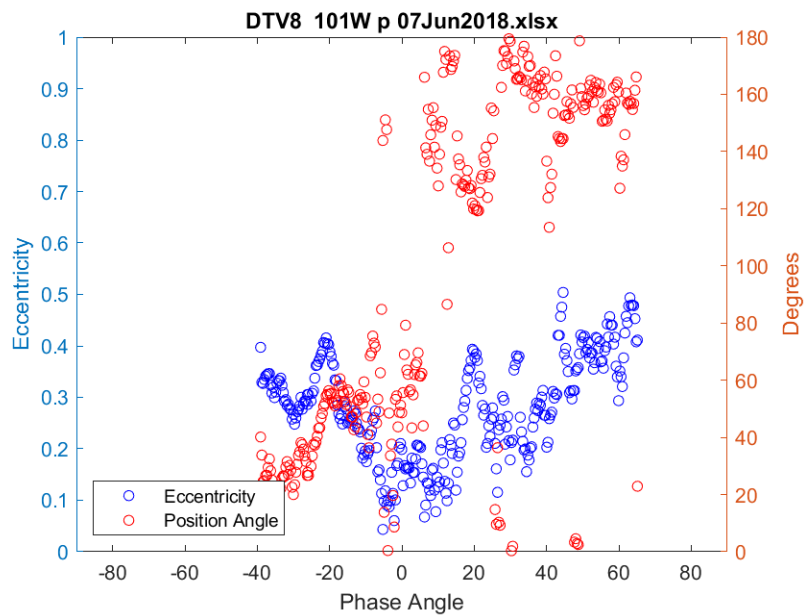


**Figure A.51** DirecTV 8 eccentricity and position angle for 7 June 2018

# Bibliography

Moody, J., Gregory, S., & Milster, S. 2018, Polarization Signatures For Geo Satellites, Tech. Rep. 1, Air Force Research Laboratory, Kirkland AFB

Pasqual, M., Cahoy, K., & Hines, E. 2015, Active Polarimetry for Orbital Debris Identification, Tech. rep., Advanced Maui Optical and Space Surveillance Technologies Conference, Kihei, Maui

Polo, M., Alenin, A., Vaughn, I., & Lambert, A. 2016, GEO Satellite Characterization through Polarimetry using Simutaneous Observations from nearby Optical Sensors, Tech. rep., Advanced Maui Optical and Space Surveillance Technologies Conference, Kihei, Maui

Stryjewski, J., Tyler, D., Roggemann, M., & Peterson, N. 2010, Real Time Polarization Light Curves for Space Debris and Satellites, Tech. rep., Advanced Maui Optical and Space Surveillance Technologies Conference, Kihei, Maui

# Index

Ellipticity, 21

GOLDS catalog, 8

Light curves, 4

Phase angle, 3

Photometry  
    definition, 3

Polarimetric fraction ringing, 35

Polarimetry  
    definition, 3

Position angle, 21

Stokes Parameters

$S_1$ , 21

$S_2$ , 21

    definition, 7